Case studies applying a wellbore-proppant simulator in the Midland Basin, Montney, and Bakken Shale Plays

Chris Ponners

ResFrac Corporation

Mohsen Babazadeh

ConocoPhillips Company

Craig Cipolla

Hess Corporation

David Cramer

ConocoPhillips Company

Egor Dontsov

ResFrac Corporation

John Lassek

Hess Corporation

Ripudaman Manchanda

ExxonMobil Corporation

Michael McKimmy

Hess Corporation

Daniel Ramirez Tamayo

ExxonMobil Corporation

Mojtaba Shahri

Apache Corporation

Mark McClure

mark@resfrac.com

ResFrac Corporation

Additional Declarations: The authors declare no competing interests.

Case studies applying a wellbore-proppant simulator in the Midland Basin, Montney, and Bakken Shale Plays

Chris Ponners[1], Mohsen Babazadeh[2], Craig Cipolla[3], David Cramer[2], Egor Dontsov[1], John Lassek[3], Ripudaman Manchanda[4], Michael McKimmy[3], Daniel Ramirez Tamayo[4], Mojtaba Shahri[5], Mark McClure[1]

1. ResFrac Corporation, Palo Alto, CA; 2. ConocoPhillips Company, Houston, TX; 3. Hess Corporation, New York, NY; 4. ExxonMobil Corporation, Houston, TX; 5. Apache Corporation, Houston, TX

Corresponding author: Mark McClure (mark@resfrac.com)

Abstract

Plug and perf hydraulic fracturing is performed with high-pressure injection of fluid and proppant from perforation clusters along a wellbore. During this process, uniform placement of fluid and proppant is important for maximizing economic performance. In prior work, we developed a wellbore-proppant transport simulator, which accounts for a wide range of phenomena, including proppant suspension, proppant settling, perforation erosion, perforation pressure drop, inertial effects, perforation orientation, and random variance, among others. In the present work, we calibrate the simulator to downhole imaging measurements of perforation erosion from wells in the Midland Basin, Montney, and Bakken Shale plays. The simulator uses several empirical coefficients. We identify coefficients that have consistent values in the calibrations to all datasets. On the other hand, a few of the coefficients exhibit variability from dataset to dataset. We show how these parameters can be calibrated on a case-by-case basis prior to using the simulator for design optimization. Based on these case studies, we identified several opportunities to improve the simulator physics – by accounting for perforation 'inline' effects, including random variance in erosion coefficient, and increasing the amount of proppant suspension. Comparison across datasets shows that there is not a single consistent trend in heel-side or toe-side erosion bias. Different physical processes have opposing effects on heel/toe-side bias, and depending on the stage design and practical conditions, these processes can have different relative magnitudes. Correspondingly, the optimal perforation design varies from case-to-case, depending on which type of 'bias' is observed in the base design. The simulator predicts that measured erosion uniformity should be lower than the proppant or slurry uniformity. This result is supported by observations from a Bakken dataset in this study, where fiber-based slurry allocations yielded a significantly higher uniformity index than downhole imaging-based measurements. The implication is that the 'uniformity index' of erosion, observed from downhole imaging, cannot be taken as a direct proxy for the uniformity of proppant or fluid outflow. Finally, the simulator was applied to each field dataset to identify the optimal perforation design. The optimization procedure identified opportunities to improve the cluster-level uniformity index of proppant placement by a range of 0.12 to 0.19. Because each dataset requires case-specific calibration prior to optimization, there is no single 'best' design for all circumstances.

1. Introduction

Uniform placement of fluid and proppant is essential for efficient hydraulic fracturing in shale. Nonuniformity causes overstimulation of some areas along the lateral and understimulation of others (Kaufman et al., 2019). Cipolla et al. (2024) estimate a roughly 20% production difference between wells with high and low uniformity.

Diagnostics that provide post-job assessments of uniformity are practical, accurate, and affordable (Robinson et al., 2020; Cramer et al., 2020; Lorwongngam et al., 2020; Cramer and Friehauf, 2024; Dhuldhoya et al., 2022). Downhole imaging tools make it possible to measure perforation erosion, enabling estimates for where proppant flowed from the well (Robinson et al., 2020; Cramer et al., 2020; Cramer and Friehauf, 2024). Fiber optic measurements provide cluster-by-cluster flow allocations (Dhuldhoya et al., 2022; Lorwongngam et al., 2020).

If we can measure uniformity, we can optimize it. Many strategies for maximizing uniformity are low cost and straightforward to implement. Design parameters that affect uniformity include: (a) shots per cluster, (b) initial perforation diameter, (c) perforation phasing, and (d) random variance in perforation gun performance (Dontsov et al., 2024; Cramer et al., 2024). Stage length, cluster spacing, and clusters per stage also play a major role; however, these parameters are convolved with the broader optimization of well spacing and fracture design (McClure et al., 2023).

Limited-entry completion is now widely adopted to increase uniformity (Lecampion et al., 2015; Weddle et al., 2018; Cramer et al., 2020; Lorwongngam et al., 2023). If injection did not include proppant, then uniformity would have a simple, monotonic relationship with perforation pressure drop – more is better. However, with proppant, the process is more complicated. Proppant inertia and gravitational settling cause proppant placement to be less uniform than slurry placement. Further, proppant erodes perforations, degrading uniformity over time. Designs with extreme limited-entry may experience more non-uniform erosion, paradoxically resulting in lower uniformity (McClure et al., 2024).

Correlations and/or physics-based simulators can be used to help optimize design. A large amount of experimental and numerical modeling work has been performed to characterize the key processes affecting proppant transport from the wellbore (Gruesbeck and Collins, 1982; Gillies, 1993; Wu and Sharma, 2016; Ngameni et al., 2017; Wu, 2018; Ahmad and Miskimins, 2019a; Ahmad and Miskimins, 2019b; Ahmad, 2020; Ahmad et al., 2021; Liu at al., 2021; Sinkov et al., 2021; Snider et al., 2022; Wang et al., 2022). How do we integrate this information into a practical methodology for optimizing perforation cluster design?

There is no substitute for field data. It is impossible to perfectly reproduce practical in-situ conditions in experiments and modeling. Furthermore, differences in casing grade and manufacturing, sand supply, fluid formulation, cementing practices, in-situ stress, and other factors affect the details of proppant transport. Because of these complicating factors, there is no single correlation or rule of thumb that is applicable in all contexts.

In this paper, we propose a practical engineering workflow integrating field data with a comprehensive physics-based simulator. Dontsov (2023) reviewed the literature and derived a set of equations capable of describing the breadth of proppant transport results available in the literature. In the present work, we apply the Dontsov (2023) model to field datasets and calibrate to observations with a small number of tuning parameters (discussed in Section 2.5). Differences in calibration parameters between datasets occur because of differences in casing, proppant, cement quality, and other factors. Once the model has been tuned to a well, it can be applied to other similar wells from the same operator, within the same geographic region.

The newly developed workflow has been applied to a wide variety of practical field datasets. With each application, we think critically about the process, and ask: (a) does the data exhibit patterns that we can

generalize and improve the speed and reliability of the process, and (b) does it appear that the model is missing any key physics, causing systematic discrepancies?

Based on these comparisons, in this paper, we present three modifications to the original Dontsov (2023) model: (a) the effect of inline perforation phasing, (b) the effect of random, spatially correlated variability in perforation erosion coefficient, and (c) an adjustment factor for the suspension of proppant in the well. With these additions, we apply the model to field datasets from the Bakken, Montney, and Midland Basin, and discuss similarities and differences between the observations.

2. Methods

2.1 Overview

The wellbore dynamics simulator that is used for this study focuses on fluid and proppant transport in the wellbore, outflow through perforations, and perforation erosion. The primary features of this simulator are described in detail by Dontsov (2023) and Dontsov et al. (2023). For inputs, the simulator requires: (a) the pumping schedule, (b) the number of clusters, (c) cluster spacing, (d) the number of perforation shots, (e) designed (and/or actual) shot diameter, and (f) phasing. Explicit time-stepping is employed to track progressive changes in fluid outflow, proppant outflow, and perforation erosion. The model includes the effect of perforation pressure drop, near-wellbore tortuosity, fracture-to-fracture stress shadowing, stress shadowing from the prior stage, proppant inertia, proppant gravitational settling in the wellbore, random variability in perforation phasing and initial diameter, the effect of wellbore fluid velocity on erosion, and a variety of other physical processes. To account for random variability, the tool performs Monte Carlo uncertainty quantification and generates a distribution of possible outcomes.

In the present work, we add three new processes to the model: (a) a correction for particle suspension, (b) a correction for the effect of inline perforating, and (c) variability in the perforation erosion coefficient.

2.2 Suspension adjustment

Upon broad comparison of results with field data, it is apparent that in cases with higher mesh proppant, particles are suspended better than anticipated by the original correlation from Dontsov (2023). There are several likely causes. First, the calibration of suspension flow was performed with datasets using relatively large particles (i.e. not 100 mesh proppant). Second, the calibration was based on laboratory experiments with water, while typical hydraulic fracturing fluids contain additives, such as friction reducers, which can alter the behavior of the fluid, especially for turbulent flow.

To compensate for this lack of certainty, a suspension calibration parameter S is introduced. Consequently, the dimensionless gravity (G) and settling time (t_o) (defined by Dontsov, 2023) are calculated as:

$$G = \frac{8\phi_m(\rho_p-\rho_f)gd_w}{Sf_D\rho_f v_w^2}, \qquad t_0 = \frac{9\mu_a d_w S}{2(\rho_p-\rho_f)ga^2}, \qquad (1)$$

where ϕ_m is the maximum volume fraction of particles, ρ_p is the density of the particle grains, ρ_f is the density of the fluid, g is the gravitational constant, d_w is wellbore diameter, f_D is the numeric constant, v_w is the average flow velocity in the wellbore, μ_a is apparent viscosity, and a is the proppant radius. As can be seen from this change, the parameter S effectively reduces the density contrast and thus alters the ability of particles to be suspended. For S greater than 1.0, the particles are suspended better. As discussed in Section 4.2, the optimal choice of S depends on particle size.

The dimensionless gravity parameter quantifies the level of proppant asymmetry in the wellbore. If the parameter is very small, on the order of one or less, then particles are perfectly suspended. By contrast, if this parameter is large, such as on the order of a hundred, then there is a strong asymmetry and the flowing bed is practically formed in the wellbore. Transitioning from 1 to 100, the distribution of proppant becomes increasingly asymmetrical towards the bottom of the wellbore. As can be seen from the definition of G, it strongly depends on average flow velocity in the wellbore. In the heel part of the stage, its magnitude is relatively small, and particles are well suspended. At the same time, towards the toe part of the stage, the velocity drops and particles start to settle. The time scale t_0 is an apparent settling time. Once a perforation cluster is encountered and the average wellbore velocity is reduced, it takes some time or flow distance for the flow to reach a new equilibrium. More details can be found in the paper Dontsov (2023).

2.3 Inline adjustment

In computational fluid dynamics simulations, Liu et al. (2021) and Wang et al. (2022) observed that if all the perforations within a cluster are located 'inline' (i.e. they have the same phasing), then the toe-side shots receive more proppant. The amount of proppant increases for downstream inline perforations within the same cluster. In other words, if they are inline, the second perforation in a cluster takes more proppant than the first one, the third perforation takes even more than the second one, etc. As discussed in Section 4.1, this modeling prediction from Liu et al. (2021) and Wang et al. (2022) is supported by the field datasets that we reviewed in this study.

Because of proppant inertia, some of the particles are unable to fully turn into the first perforation and consequently miss it. As a result, such particles tend to elevate concentration locally at the given perforation azimuth. If the next perforation has the same phasing, then it receives more proppant because of the local concentration of proppant created by 'missing' the previous shot. The process repeats for subsequent inline perforations.

Figure 1 shows a schematic of the inline process. The dashed lines show the 'ingestion zones,' or the regions where proppant will successfully flow into each perforation. The dark gray zone shows how there is some larger zone in the wake of a perforation where proppant concentration is temporarily elevated, and which can impact the flow into subsequent inline shots.
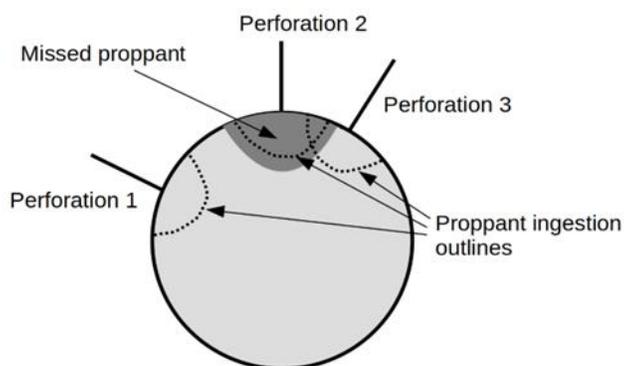

Figure 1: Wellbore cross-section illustrating the effect of inline perforations. The dark gray zone indicates an elevated particle concentration due to an outflow into a vertically oriented perforation. Perforations 1, 2, and 3 show the potential overlap of this high particle concentration with the corresponding ingestion zones.

Proppant concentration is elevated downstream of the vicinity of perforation shots because: (a) some grains miss the shot due to inertia, and (b) the outflow of fluid from the shot pulls proppant inward from across the rest of the wellbore. As a consequence, perforation shots that are immediately downstream of

another shot (with similar phasing) will tend to accept an elevated amount of proppant. To account for this 'inline' effect, we introduce an additional fitting parameter.

To calculate particle concentration in the missed zone, let η be the turning efficiency into the perforation. This allows us to calculate particle concentration in the missed zone as:

$$\Delta\Phi = I_c \frac{1-\eta}{\eta} \frac{q_p^p}{q_s A_m},$$ (2)

where I_c is the inline correction multiplier, q_p^p is proppant flow rate through perforation, q_s is the slurry flow rate in the wellbore after the perforation, and A_m is the area occupied by the missed proppant.

After each shot, the proppant distribution eventually returns to its undisturbed equilibrium position, and so the concentration of particles in the inline zone decreases with time with the time scale defined by:

$$t_{inline} = \frac{9\mu_a d_w^2}{2a^2 \rho_f v_w^2}.$$ (3)

Generally, the inline effect is strong for shots within the same cluster but is nearly nonexistent from cluster to cluster. It tends to increase in magnitude from the second to third or fourth inline shot within a cluster.

In the model, the "missed proppant" is calculated for every perforation shot, based on its orientation and the amount of missed particles. The phasing of the missed shot affects the size and location of the inline zone downstream. Three hypothetical examples are shown in Figure 1. First is the case in which the next perforation has a sufficiently different azimuth (Perforation 1). In the second case, the next perforation is perfectly aligned with the initial perforation (Perforation 2). Finally, in the last case the downstream perforation is slightly offset from the initial perforation (Perforation 3). The ingestion zones or the zones from which proppant flows into these respective perforations are shown by the dashed lines. In the case of Perforation 1, there is no overlap between the ingestion zone and the missed proppant (or the dark gray area), and hence there is no effect. For the second case, in which the downstream perforation is perfectly aligned with the previous one (Perforation 2), the effect is maximized and all the proppant that missed the initial perforation enters the next hole. If there is a slight offset with the next perforation, then the overlap area is calculated and the inline effect is reduced (Perforation 3). The magnitude of the elevated concentration defined in Equation 2 as well as the degree of overlap discussed above determine the final result for the 'inline correction.'

2.4 Random variance in erosion coefficient

As shown in Section 3, field observations of perforation erosion are highly variable from stage to stage, even when there is a clear trend "on average." Simulations incorporating random variance in perforation phasing and initial diameter do not capture the magnitude of the random variance. To account for the remaining variance, we include random variability in the erosion coefficient, α.

The erosion model adopted in this study can be summarized as follows:

$$\frac{dD_d}{dt} = \alpha C(v^2 + \gamma V^2), \frac{dD_u}{dt} = \alpha C v^2, \frac{dD_s}{dt} = \alpha C v^2,$$ (4)

where in the above equation, C is proppant concentration, v is the average flow velocity through perforation, V is the average flow velocity in the wellbore, D_d is the perforation size in the downstream direction, D_u is the perforation size in the upstream direction, while D_s is the perforation size perpendicular to the flow in the wellbore. The term with the erosion multiplier captures the effect of wellbore flow on the erosion and is primarily responsible for the heel bias that is often observed in the field.

Variance in the erosion coefficient may have several possible causes. First, there may be variability in steel quality or stress state between or within casing strings. Second, the quality of cement behind casing can be spatially variable. Lower quality cement will promote flow behind casing and elevate the erosion from the outer side. Third, there may be local variability in rock formation properties immediately behind casing, which will alter initiation and flow. Finally, there is a positive feedback loop – shots that erode the most take more fluid, encouraging further erosion.

Observations suggest that there is a spatial correlation, i.e. zones with high level of erosion tend to be relatively localized within a certain distance within a stage. In order to model this phenomenon, we introduce uncertainty in the perforation erosion process by specifying an erosion multiplier for each individual perforation:

$$\alpha_m = \frac{1 + 10^{\alpha_u}}{\langle 1 + 10^{\alpha_u} \rangle},$$

(5)

where α is the erosion constant that increases the overall rate of erosion (Cramer, 1987; Long et al., 2015; Dontsov et al., 2023), while α_u is the corresponding uncertainty that is calculated from the multivariate normal distribution. The erosion multiplier is normalized by its average value (as shown in the denominator term with the triangular brackets) to ensure that the uncertainty does not change the overall rate of erosion. The latter multivariate normal distribution incorporates the effect of spatial correlation via the covariance matrix, whose entries are calculated using spherical model for variogram as

$$M_{ij} = (\sigma_R^2 - \sigma_0^2)\left(1 - \frac{3d_{ij}}{R} + \frac{d_{ij}^3}{2R^3}\right), \qquad M_{ii} = \sigma_R^2,$$

(6)

where d_{ij} is the distance between ith and jth perforations. When $d_{ij}/R > 1$, then $M_{ij} = 0$.

Overall, the random variance in erosion coefficient is quantified by three parameters: (a) normalized standard deviation at distance zero, σ_0, (b) the normalized standard deviation at the specified distance called range, σ_R, and (c) the range, R. In variogram terminology, σ_0^2 is the 'nugget,' and σ_R^2 is the 'sill.'

2.5 Overall modeling workflow

Calibration to field data is important because field datasets show significant variability from case to case. For example, we observe that the erosion alpha parameter (Equation 4), which broadly captures the proportionality between erosion and proppant outflow, varies over a factor of at least 3x between datasets. This indicates that – holding the amount of proppant constant – some datasets exhibit much more erosion than others. In theory, it might be possible to predict this variability from analysis of steel quality, sand mineralogy, and other parameters. In the present work, we utilize a practical workflow based on calibration to data, followed by optimization.

Prior to using the model, we recommend analyzing the data to develop a list of 'key observations.' Start by defining groups of 'similar' stages. For example, perhaps some stages used consistent 0° phasing, and others used consistent 90/180° phasing. These two groups can be compared. In wells with highly variable phasing between stages, or within each stage, cross-plot key parameters such as erosion or uniformity index versus phasing, and check to see if a consistent trend emerges.

Next, estimate key metrics for each group (and, if applicable, differences in uniformity index between groups or based on a parameter such as average phasing in the stage): (a) stage-level uniformity index, (b) stage and cluster-level magnitude of erosion, and (c) the degree of toe bias, heel bias, or combined toe/heel bias apparent in the erosion data from the stages.

The uniformity of flow in each stage can be quantified with the uniformity index, defined as:

$$UI = 1 - \frac{\sigma}{\mu}, \qquad (7)$$

where σ is the standard deviation and μ is the mean. UI can be calculated on a per cluster or per shot basis, and it can be calculated for 'increase in effective perforation diameter,' 'increase in perforation area,' 'proppant outflow,' or 'slurry outflow.' Sometimes, uniformity index is normalized by dividing standard deviation by the square root of the number of shots or clusters in a stage minus 1. In this paper, the uniformity index is not normalized using this procedure; therefore, it is possible for values of UI to be negative.

When matching the simulation results to the 'key observations' from the data, there are several parameters that can be modified:

1. The parameter α, which scales the constant of proportionality between erosion and proppant outflow from the well (Long et al., 2015). Increasing α results in more overall erosion.

2. The parameter γ, which scales the effect of lateral fluid velocity on erosion (Dontsov et al., 2024). Increasing γ results in greater erosion towards the heel side of the stage.

3. The 'fracture net pressure,' which scales the magnitude of fracture-to-fracture stress shadowing within a stage. Increasing fracture net pressure increases fluid flow in both the toe and heel of the stage, with a reduction in outflow from the middle clusters of the stage.

4. The magnitude of stress shadow from the prior stage(s). Increasing stress shadow from prior stages reduces the amount of fluid outflow from the toe side of the stage.

Other input parameters specify: near-wellbore tortuosity, effective tensile strength (which can be randomized, and which can be used to match data where a significant percentage of clusters never breaks down), and a multiplier on the probability of perforation plugging (used to match the percentage of clusters that plug during injection).

As is described above, in the present work, we add three new processes to the model. They are:

1. An 'inline correction' multiplier, I_c, that accounts for the effect of placing multiple perforation shots in short succession, adjacent to each other.

2. Random variability in the erosion coefficient of each perforation shot, parameterized with σ_0, σ_R, and R.

3. A suspension multiplier, S, that increases the ability of proppant to remain suspended in the fluid (reduces the effect of gravity).

For these three new parameters, we seek to find good 'default' values that can be used consistently across datasets in the future, without (usually) needing to be included in the routine data calibration process. As discussed in Section 3.2.1, we found that most of the potential 'fitting' parameters could be set to the same value uniformly for all datasets.

3. Results and discussion

3.1 Generic sensitivity analysis simulations

Before analyzing specific datasets, generic sensitivity analysis simulations were performed to evaluate the effects of the newly implemented parameters – the inline perforation adjustment, the proppant settling adjustment, and the random variance in erosion coefficient. These simulations are not based on any particular dataset; instead, they are used to demonstrate the effect of varying model parameters.

The settings used in Simulation 1 are shown in Table 1. The design is typical for a slickwater fracturing treatment. There are three shots per cluster, each at 0° phasing, and with a 20 ft cluster spacing. The 'design' initial shot diameter is 0.4''. However, because of the zero degree phasing and the offset between the gun and the top of the well, the actual initial shot diameter averages 0.284'' (Bell, 1987). For each simulation, 500 Monte Carlo draws are performed for uncertainty in phasing, shot diameter, effective tensile strength, and (if applicable) erosion coefficient.

Table 1: Settings used in Simulation 1.

Injection rate	90 bpm	Perf phasing	0°
Max prop conc	2.25 ppa	Cluster spacing	20 ft
Proppant mesh	100	NW dP coefficient	200 psi/bpm^0.5
Stage length	200 ft	Str shadow prior stage	1500 psi
Casing ID	4.8"	Fluid type	Slickwater
Initial shot diam	0.284"	Shots per cluster	3
Erosion alpha mult	1	Phasing STD (stage)	10°
Erosion gamma mult	1	Phasing STD (perf)	10°
Eff tensile str	500 psi	Initial diam STD	0.02"
Tensile str STD	500 psi	Single frac net pres	200 psi

Figure 2 shows the cumulative proppant outflow per cluster and per shot, the cumulative slurry outflow per cluster, and the ratio of final diameter to initial diameter. In the simulation, erosion and proppant outflow have a general heel bias, caused by: (a) the effect of horizontal fluid velocity on erosion (Equation 4), and (b) gravitational settling of proppant as velocity decreases near the toe (Dontsov et al., 2024). Other relevant effects include: (a) limited-entry pressure drop, (b) near-wellbore pressure drop, (c) proppant inertial effects causing proppant to 'miss' the shots at high velocity, (d) stress shadow from the prior stage, and (e) stress shadow from fractures within the same stage.

Despite the overall heel bias, there is a large outflow from the well in the final perforation shot (Figure 2). In the simulation, this occurs primarily because of gravitational effects – the tendency of proppant to

settle in the toe-side stages and 'miss' the perforation shots at the top of the well. All remaining proppant must outflow when it reaches the final shot, creating a large outflow at the toe.

This simulation result has a sound physical basis. However, comparison with field data shows that it exaggerates the effect of gravity and the magnitude of proppant outflow at the toe-side shot, at least for designs with 100 mesh proppant.
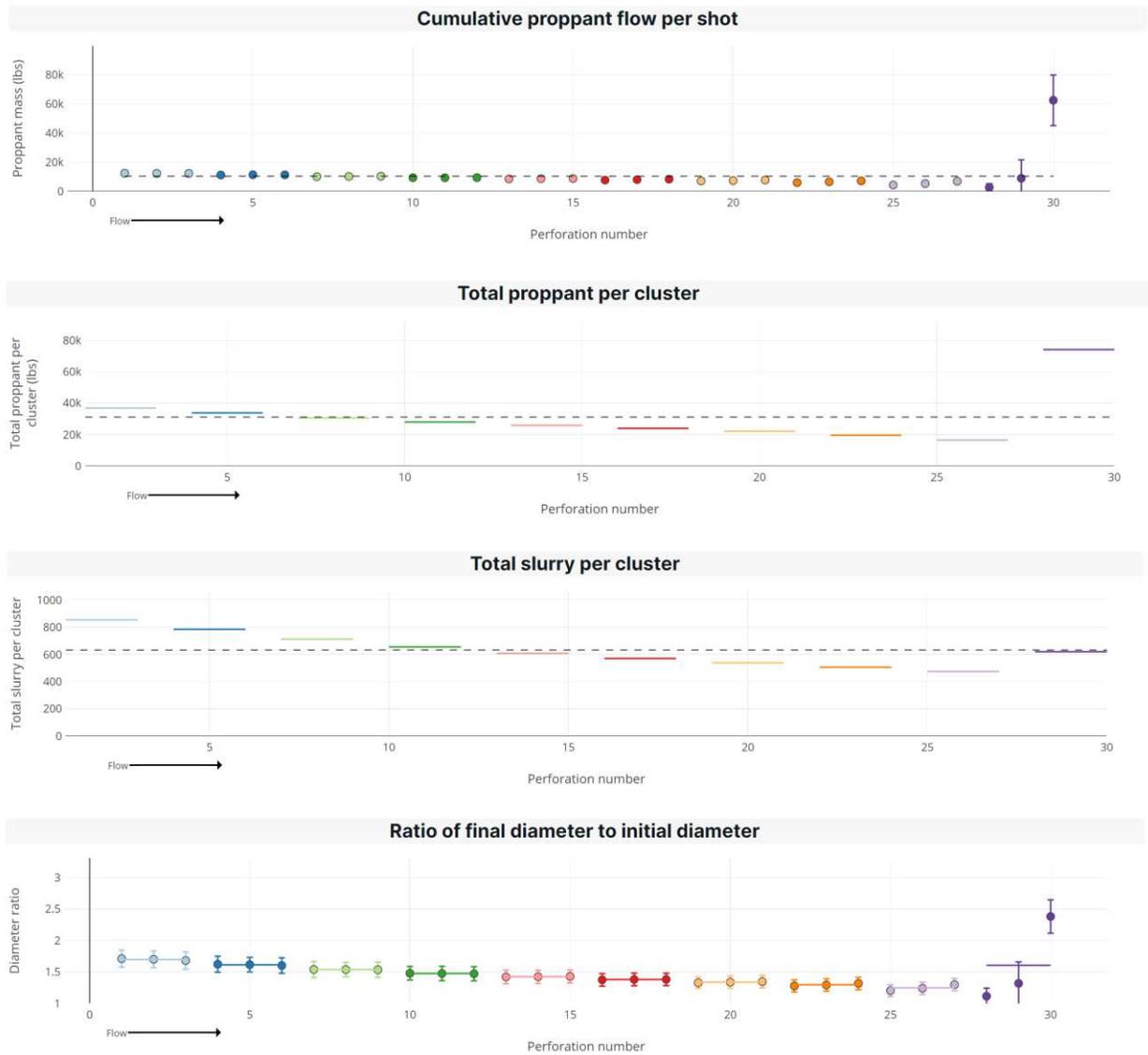

Figure 2: Results from Simulation 1, which does not use any of the new updates to the physics parameters. Each dot shows the 'per-shot' results, and the whiskers show the P10/P90 ranges. The horizontal lines show the 'per-cluster' results. The shots in each cluster are plotted with separate colors. The horizontal dashed lines show the overall average.

To reduce the effect of settling, Figure 3 shows a simulation with the 'suspension factor' set to 10 (Equation 1). As discussed in Section 2.2, this adjustment increases the resistance of the proppant to gravitational settling. The final cluster still takes more proppant, but the effect is much less pronounced than in Figure 2, with 20,000 lbs of proppant in the final shot, instead of 60,000 lbs, and with a diameter increase of 65% instead of 140%.
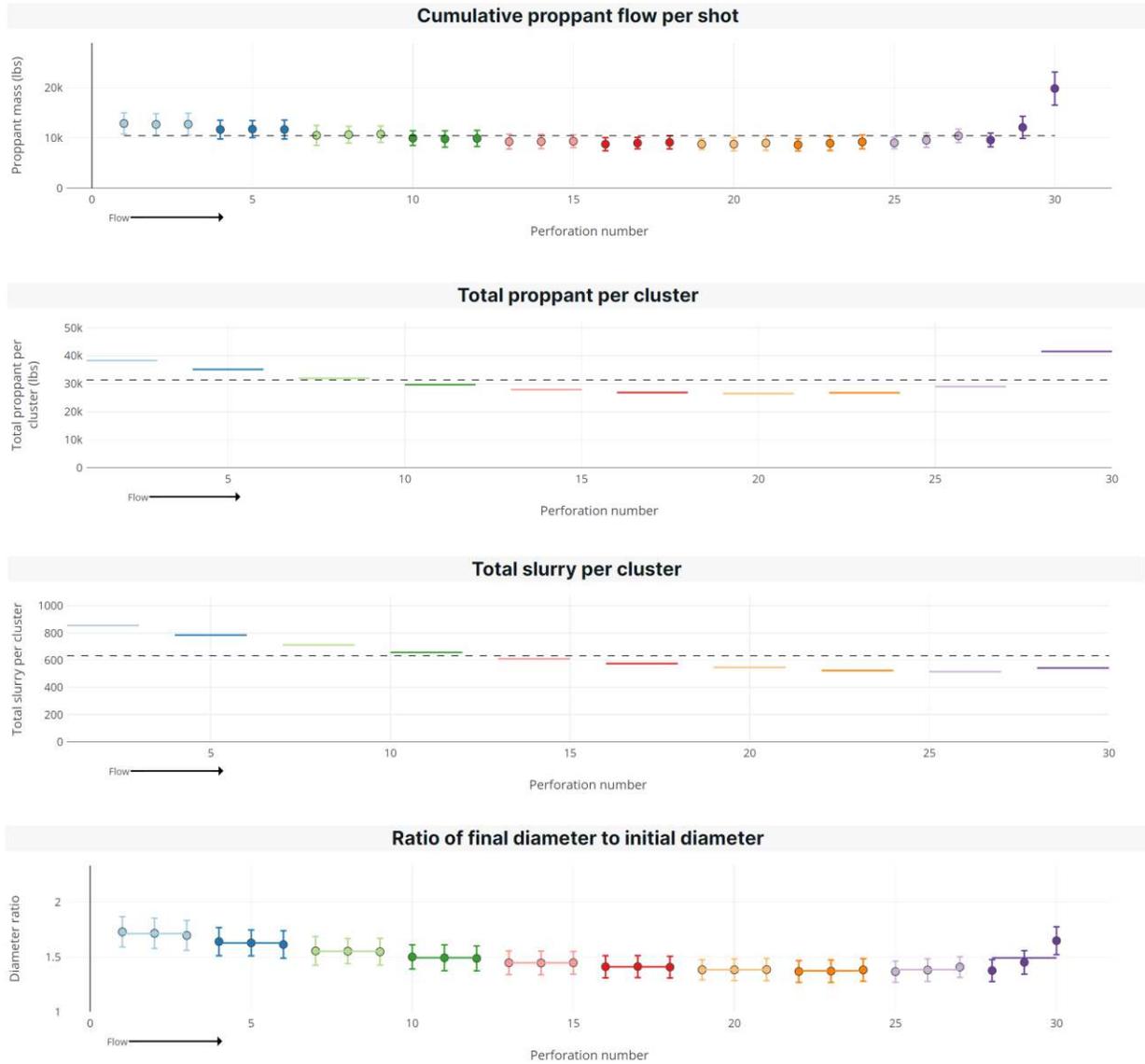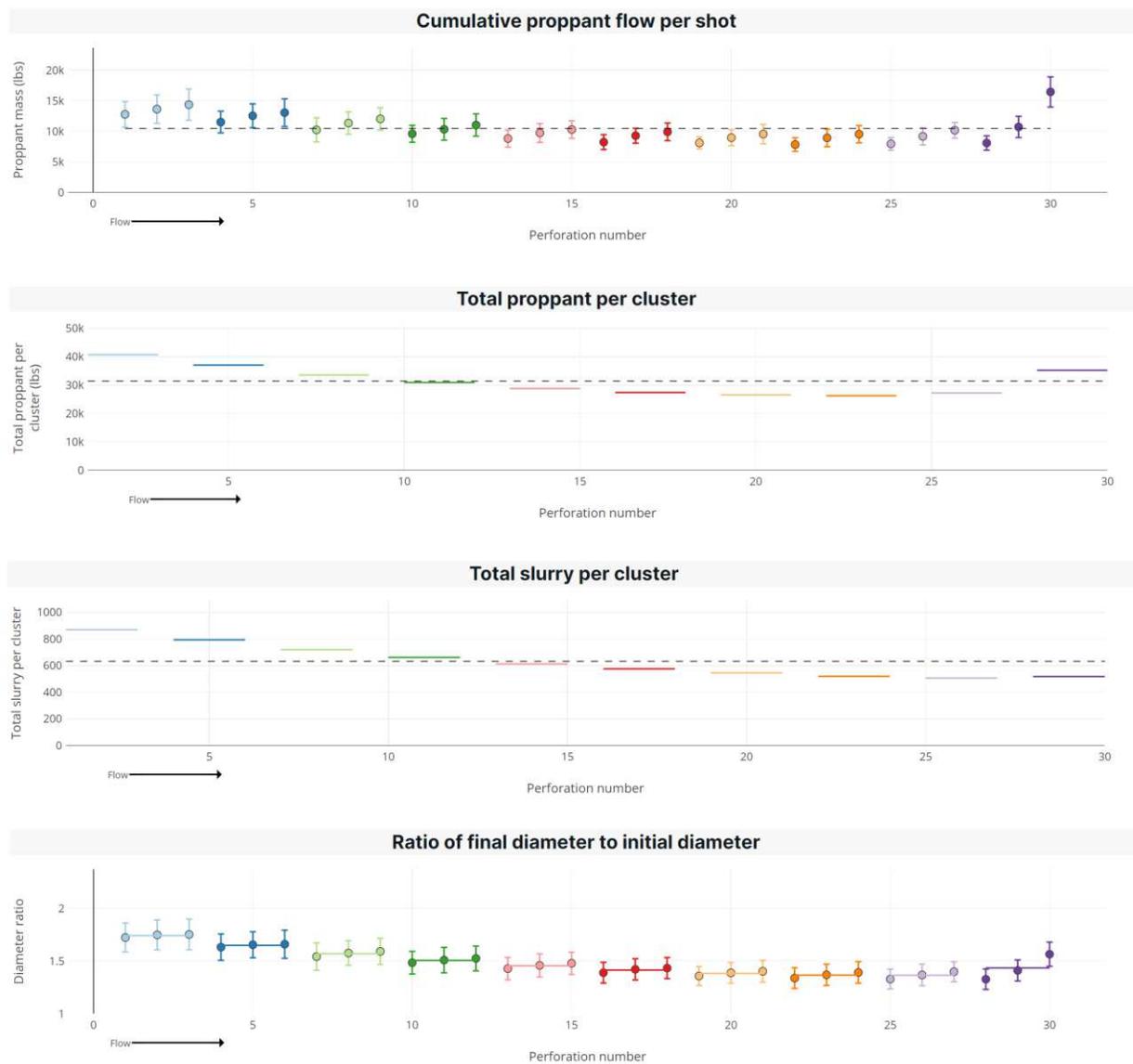
Figure 3: Results from Simulation 2, with suspension multiplier set to 10. Each dot shows the 'per-shot' results, and the whiskers show the P10/P90 ranges. The horizontal lines show the 'per-cluster' results. The shots in each cluster are plotted with separate colors. The horizontal dashed lines show the overall average.

To demonstrate the effect of the 'inline' adjustment (Section 2.3), Simulation 3 has the suspension multiplier set to 10.0 and the 'inline adjustment' activated with a multiplier of 1.0 (Figure 4). Now, there is a tendency for the third shot in each cluster to take the most proppant, and the first shot to take the least. The inline process weakens the effect of gravity on outflow because the second and third shots preferentially accept proppant that misses the first shot in each cluster.

Figure 4: Results from Simulation 3, with suspension multiplier set to 10 and inline adjustment set to 1.0. Each dot shows the 'per-shot' results, and the whiskers show the P10/P90 ranges. The horizontal lines show the 'per-cluster' results. The shots in each cluster are plotted with separate colors. The horizontal dashed lines show the overall average.

Figure 5 shows results from Simulation 4, which is the same as in Figure 4, but also with random variability in the erosion coefficient, as given by Equations 5 and 6. The nugget is set to 0.18; the sill is set to 0.25; and the range is set to 50 ft.
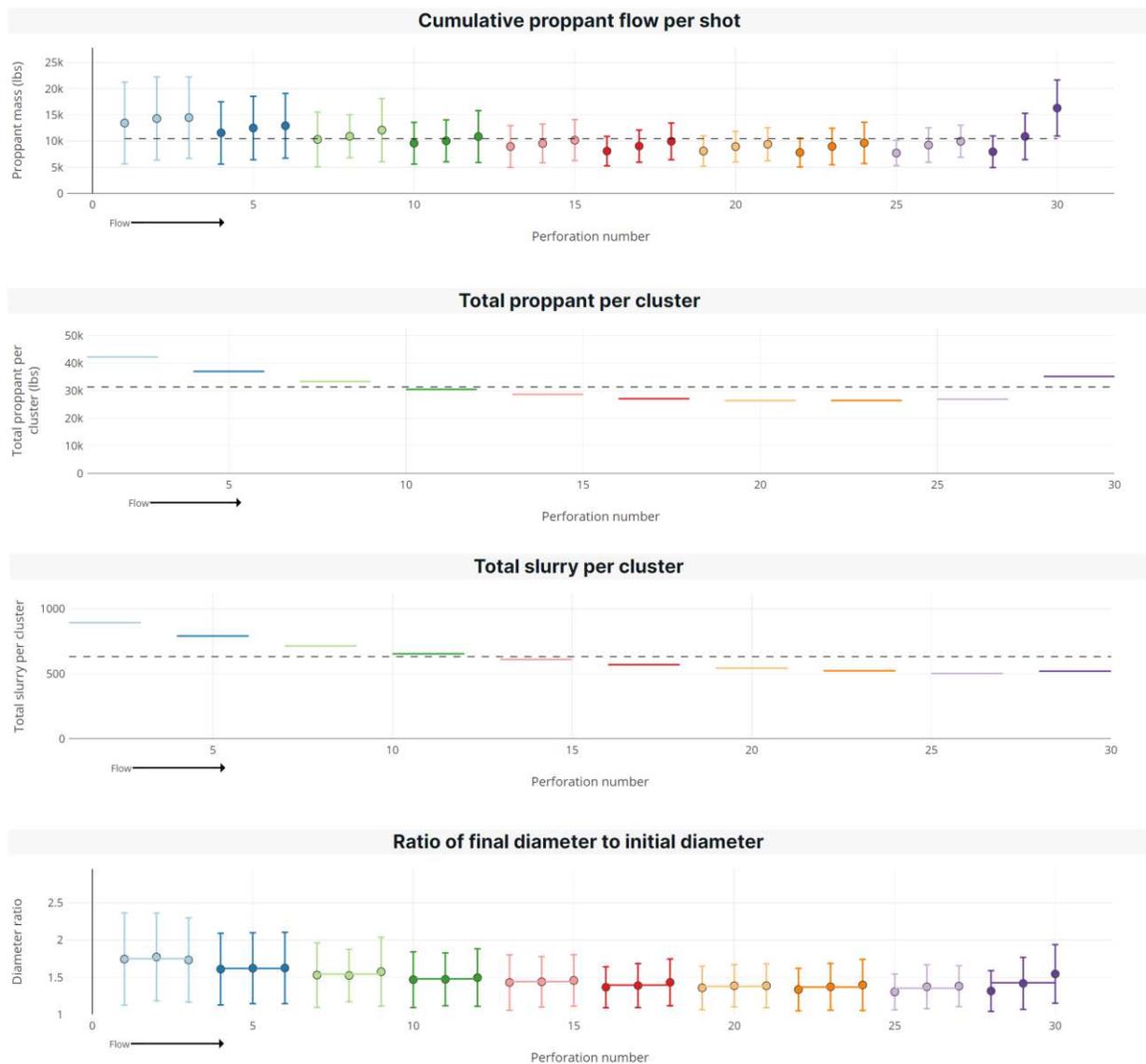
Figure 5: Results from Simulation 4, with suspension multiplier set to 10, inline adjustment set to 1.0, and spatially correlated random variance in erosion coefficient. Each dot shows the 'per-shot' results, and the whiskers show the P10/P90 ranges. The horizontal lines show the 'per-cluster' results. The shots in each cluster are plotted with separate colors. The horizontal dashed lines show the overall average.

Comparing Figure 5 with Figure 4, the average erosion and outflow results are fairly similar. However, the uncertainty bars on the per-cluster proppant flow and erosion are much wider. Figure 6 shows the per-cluster erosion profiles for four individual Monte Carlo draws from Simulation 4. In keeping with the overall 'average' trend, there is a tendency for a heel bias. However, because of the log-normal random variability in erosion, individual draws often show deviation from the trend, with more erosion in the middle or toe of the stage. This model result is realistic – in actual field datasets, there is strong variability from stage to stage, and individual stages often deviate entirely from the overall statistical trend.
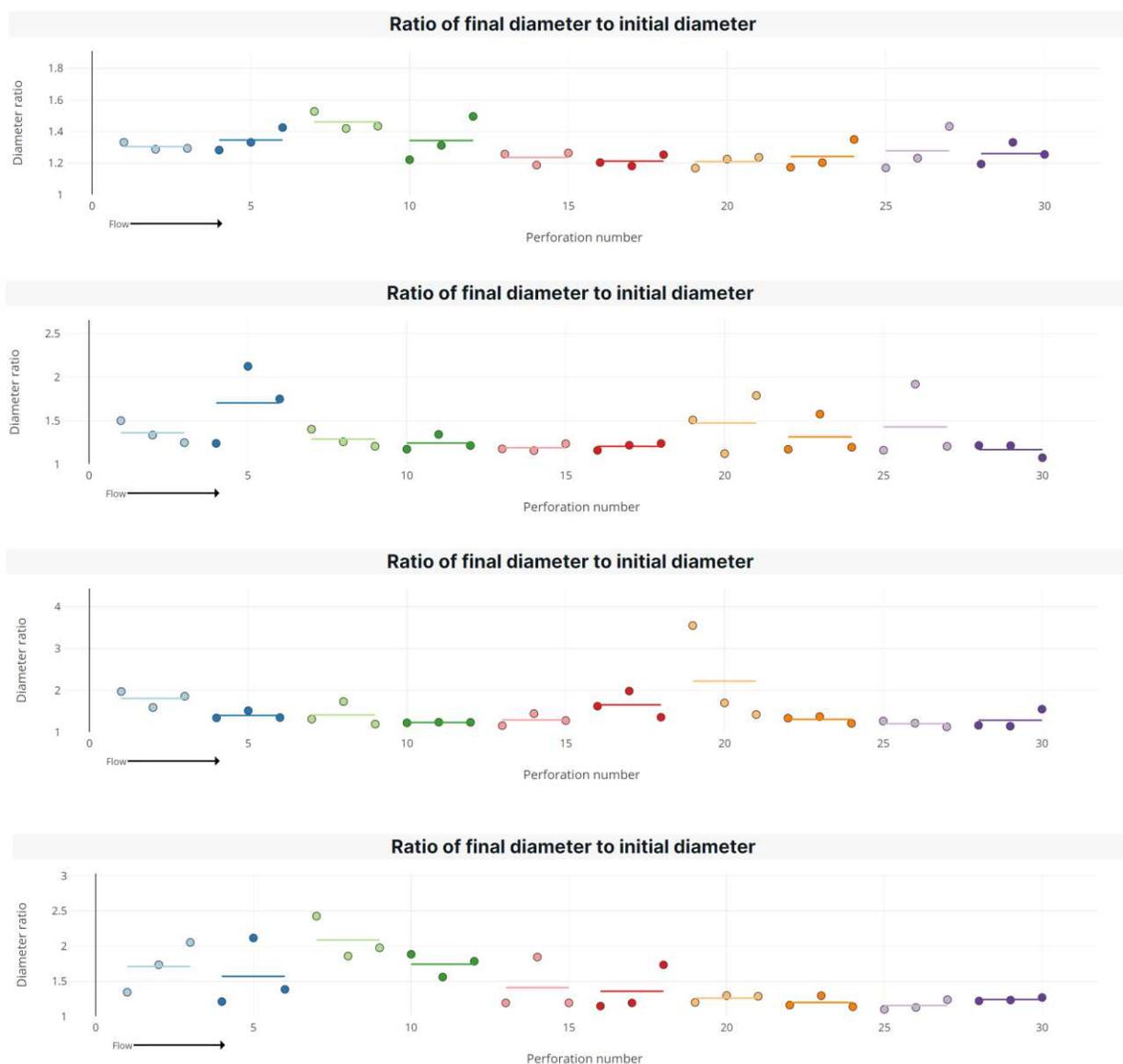
Figure 6: Individual stages from Monte Carlo draws during Simulation 4, which includes random variance in erosion coefficient. Each dot shows the 'per-shot' results, and the whiskers show the P10/P90 ranges. The horizontal lines show the 'per-cluster' results. The shots in each cluster are plotted with separate colors.

For comparison, Figure 37 shows the shot-by-shot erosion profile measured in several stages from the Bakken plug and perf dataset. The stage-to-stage variability has similar magnitude as shown in Figure 6.

Figure 7 shows the distribution of per-cluster proppant uniformity index across the 500 Monte Carlo draws for Simulations 3 and 4 (with and without log-normal variability in erosion coefficients, corresponding to the results in Figure 4 and Figure 5). The average UI is modestly lower in Simulation 4. However, there are far more stages with poor uniformity in the case that includes variability in erosion coefficient. This is a more realistic result. For example, Figure 8 shows the observed distribution of erosion uniformity index from the MPP Well 3 dataset.
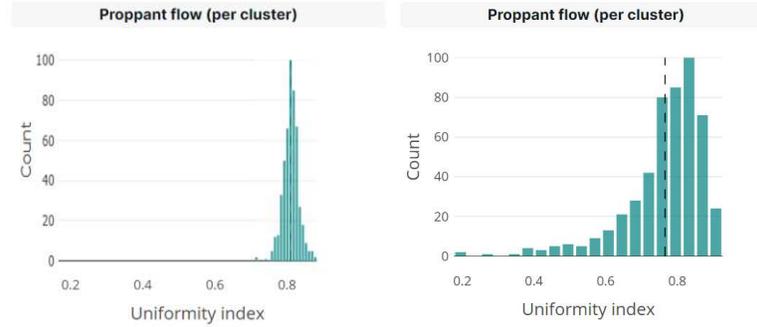
Figure 7: Distribution of uniformity index for the sims 3 (Left) and 4 (right), without and with log-normal variability in erosion coefficients. The dashed vertical line shows the overall average.
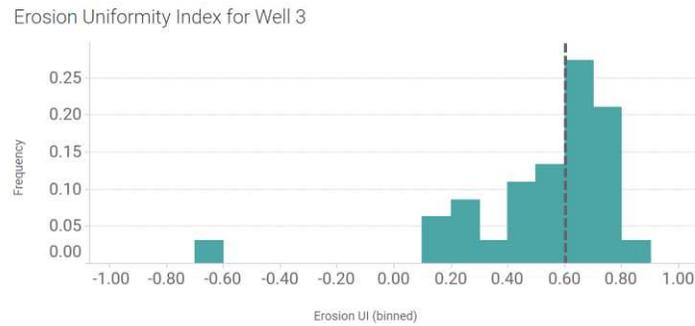

Figure 8: Distribution of uniformity index for 34 stages from the MPP Well 3 dataset. The dashed vertical line shows the overall average.

In Section 3.2, we present model matches to fifteen field datasets. Figure 9 shows results from Simulation 5, a generic simulation using model parameters broadly similar with the matches in Section 3.2. They are: (a) alpha multiplier set to 0.6, (b) gamma multiplier set to 0.1, (c) suspension factor set to 10.0, (d) inline correction factor set to 3.0, (e) sill set to 0.3, nugget set to 0.15, and range set to 200 ft, (f) individual fracture net pressure set to 200 psi, and (g) stress shadow from the previous stage set to 300 psi. With these settings, the inline effects are pronounced, there is a relatively flat distribution across the stage, with neither toe nor heel bias.
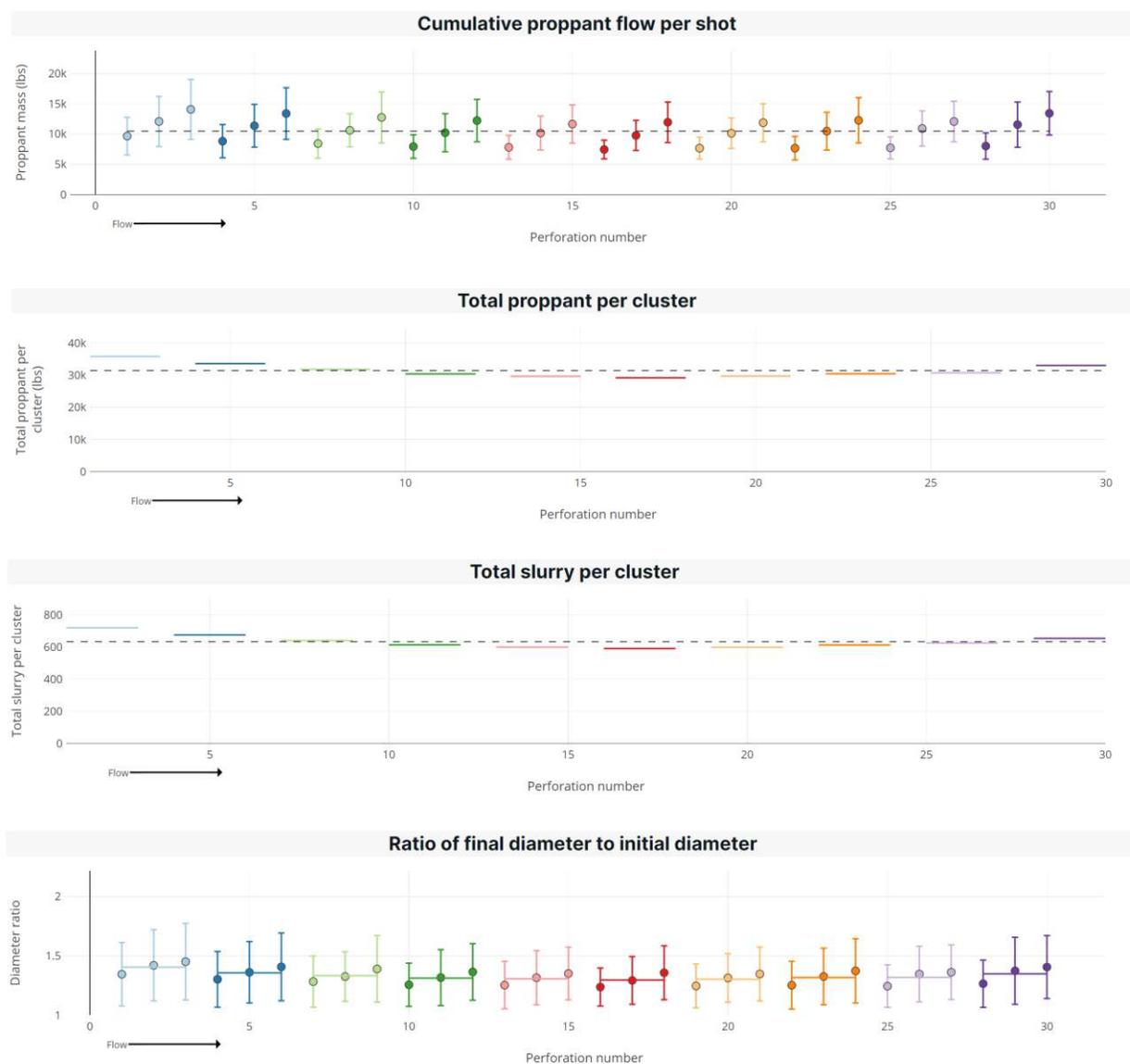
Figure 9: Using similar parameters as the field data matches in Section 3.2. Each dot shows the 'per-shot' results, and the whiskers show the P10/P90 ranges. The horizontal lines show the 'per-cluster' results. The shots in each cluster are plotted with separate colors. The horizontal dashed lines show the overall average.

3.2 Case studies

3.2.1 Overview of the datasets

We reviewed downhole imaging data from fifteen different stage designs, including three Montney wells (seven different designs), one Permian well (five different designs), and one Bakken well (three different designs). Table 2 provides key statistics for the fifteen designs.

All but one used a plug-and-perf design. Some of the wells had cemented fiber, and so the perforation phasing varied between stages so that the perforations could be shot in the direction opposite the fiber (as it coils gradually around the well). In the plug-and-perf designs, shots were generally inline (consistent phasing, albeit with random variance) within each stage. The sliding sleeve well used eight shots in each 'cluster,' as shown in Figure 10. In the sliding sleeve design, the shots were machined to have consistent

diameter and were all located at precisely the same MD along the well (instead of being placed sequentially after each other, which would be more common).

Table 2: Summary of key design statistics for the fifteen stage designs that were analyzed.

| Basin	Design Name	Stage Count	Avg Phasing (Gun)	Stage Length	Cluster #	Cluster Spacing	Average SPC	Taper Design?	Phasing	Orientation	Max Rate	Fluid /ft	Proppant /ft	Fluid System	Proppant Type
Montney - P&P	Well 3 – 5x3 Top	16	8	200	5	40	3.00	No	Inline	Top	90	40	3067	Slickwater	40/140M
Montney - P&P	Well 3 – 5x4 Top	18	8	200	5	40	4.00	No	Inline	Top	100	40	3067	Slickwater	40/140M
Montney - P&P	Well 4 – 8x3 Top	9	9	315	8	40	3.00	No	Inline	Varied (-50 to 125 deg)	100	34	3080	Slickwater	100M
Montney - P&P	Well 4 – 8x3 Side	8	72	315	8	40	3.00	No	Inline	Varied (-50 to 125 deg)	100	34	3080	Slickwater	100M
Montney - P&P	Well 4 – 8x2 Top	6	16	315	8	40	2.00	No	Inline	Varied (-50 to 125 deg)	83	34	3080	Slickwater	100M
Montney - P&P	Well 4 – 8x2 Side	2	36	315	8	40	2.00	No	Inline	Varied (-50 to 125 deg)	83	34	3080	Slickwater	100M
Montney - Sliding Sleeve	Well 2	3	-	146	3	49	8.00	No	45 deg colocated	Varied	90	37	2492	Slickwater	100M
Permian	Well 1 – 100ft Side	5	62	100	4	25	7.50	Tapered (7,7,8,8)	Inline	Varied	90	48	2000	Slickwater	100M
Permian	Well 1 – 200ft Side	4	60	200	8	25	3.75	Tapered (3,3,4,4,4,4,4,4)	Inline	Varied	90	48	2000	Slickwater	100M
Permian	Well 1 – 250ft Top	3	19	250	10	25	3.00	Tapered (3,3,4,4,4,4,4,4)	Inline	Varied	90	48	2000	Slickwater	100M
Permian	Well 1 – 350ft Top	2	16	350	14	25	2.14	Tapered (2,2,2,2,2,2,2,2,2,2,2,3,3)	Inline	Varied	90	48	2000	Slickwater	100M
Permian	Well 1 – 350ft Side	2	45	350	14	25	2.14	Tapered (2,2,2,2,2,2,2,2,2,2,2,3,3)	Inline	Varied	90	48	2000	Slickwater	100M
Bakken	Well 1 - 18x1 Bottom	4	226	350	18	18	1.00	No	Inline	Varied	103	34	1368	Slickwater	40/70M; 100M
Bakken	Well 1 - 17x1 Side	7	262	332	17	18	1.00	No	Inline	Varied	97	34	1368	Slickwater	40/70M; 100M
Bakken	Well 1 - 16x2 Side	3	310	320	16	18	2.00	No	Inline	Varied	91	35	1368	Slickwater	40/70M; 100M
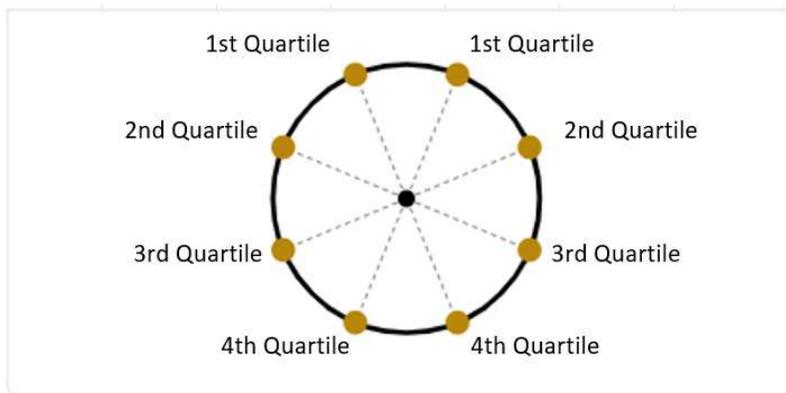
Figure 10: Configuration of the machined holes in the sliding sleeve design.

For each of the fifteen stage designs, a numerical model was set-up and matched to the field data. To the extent practical, the same model parameters were used in each match. However, the datasets did require

some individual calibration, as discussed below. Figure 11 shows the predicted versus actual uniformity index for each design, with UI measured from the increase in flow area per cluster.
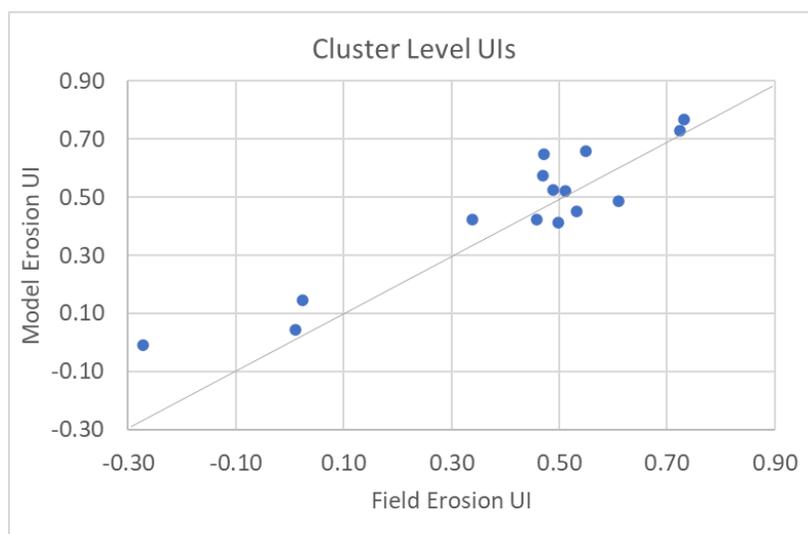

Figure 11: Cross-plot of actual versus simulated uniformity index of the percentage increase in flow area, as measured on a per-cluster basis.

Table 3 summarizes the key model parameters used to match the data. The same 'inline correction multiplier' was used in each dataset. A 'suspension multiplier' of 10.0 was used in the 100 mesh jobs and a value of 3.0 in the 40/70 jobs. The 'range' for the erosion variability was generally set to around the stage length. The nugget value was set to 0.1-0.2, and the sill was set to 0.14-0.3. Some datasets showed lower variance within each cluster but significantly higher variance between clusters; those datasets required a higher sill than nugget to capture the cluster to cluster variance. Net pressure 'per fracture' was generally set to 100-200 psi. For the plug and perf injections, α (proportional to the magnitude of erosion) varied from 0.3 to 0.8. The sliding sleeve well exhibited a substantially higher value, 1.5. The parameter γ that controls the effect of lateral velocity on erosion and was generally set to 0-0.2 (except for the sliding sleeve well).

Table 3: Key model parameters used in the match to the different datasets.

Company	Basin	Design	Stage Count	Avg Phasing (Gun)	Alpha	Gamma	Tensile Strength / Uncertainty (psi)	Net Pres (psi)	Stress Shadow (at toe, psi)	N/S/R	Inline Correction Multiplier	Suspension Multiplier
COP	Montney - P&P	Well 3 – 5x3 Top	16	8	0.8	0	700	100	100	0.2/0.35/75	3	3
COP	Montney - P&P	Well 3 – 5x4 Top	18	8	0.8	0	700	100	100	0.2/0.35/75	3	3
COP	Montney - P&P	Well 4 – 8x3 Top	9	9	0.4	0.1	800	150	100	0.15/0.30/150	3	10
COP	Montney - P&P	Well 4 – 8x3 Side	8	72	0.4	0.1	800	150	100	0.15/0.30/150	3	10
COP	Montney - P&P	Well 4 – 8x2 Top	6	16	0.4	0.1	800	150	100	0.15/0.30/150	3	10
COP	Montney - P&P	Well 4 – 8x2 Side	2	36	0.4	0.1	800	150	100	0.15/0.30/150	3	10
COP	Montney - Sliding Sleeve	Well 2	-	-	1.4	0.3	0	150	500	0.15/0.15/150	3	3
COP	Permian	Well 1 – 100ft Side	5	62	0.6	0.1	0	200	300	0.1/0.14/250	3	10
COP	Permian	Well 1 – 200ft Side	4	60	0.6	0.1	0	200	300	0.1/0.14/250	3	10
COP	Permian	Well 1 – 250ft Top	3	19	0.6	0.1	0	200	300	0.1/0.14/250	3	10
COP	Permian	Well 1 – 350ft Top	2	16	0.6	0.1	0	200	300	0.1/0.14/250	3	10
COP	Permian	Well 1 – 350ft Side	2	45	0.6	0.1	0	200	300	0.1/0.14/250	3	10
Hess	Bakken	Well 1 - 18x1 Bottom	4	226	0.3	0.2	0	150	400	0.1/0.3/294	3	10
Hess	Bakken	Well 1 - 17x1 Side	7	262	0.3	0.2	0	150	400	0.1/0.3/294	3	10
Hess	Bakken	Well 1 - 16x2 Side	3	310	0.3	0.2	0	150	400	0.1/0.3/294	3	10

Table 4 summarizes key observations from the imaging data, along with the simulated values of cluster-level UI for erosion, fluid flow, and proppant flow.

Table 4: Simulated and actual values for cluster-level erosion and uniformity index for the different datasets.

Basin	Design	Avg Gun Phasing (deg)	Per Stage Phasing Uncertainty (deg)	Per Shot Phasing Uncertainty (deg)	Target perforation diameter (in)	Actual perforation diameter (in)	Field Erosion UI	Model Erosion UI	Model Proppant UI	Model Slurry UI
Montney - P&P	Well 3 – 5x3 Top	8	5.37	5.39	0.46	0.46 @ 0 deg	0.61	0.49	0.79	0.84
Montney - P&P	Well 3 – 5x4 Top	8	6.34	6.97	0.46	0.46 @ 0 deg	0.47	0.58	0.81	0.85
Montney - P&P	Well 4 – 8x3 Top	9	6.07	7.83	0.46	0.46 @ 0 deg	0.50	0.41	0.70	0.73
Montney - P&P	Well 4 – 8x3 Side	72	19.22	11.01	0.46	0.46 @ 0 deg	0.53	0.45	0.71	0.73
Montney - P&P	Well 4 – 8x2 Top	16	9.28	9.96	0.46	0.46 @ 0 deg	0.34	0.43	0.74	0.77
Montney - P&P	Well 4 – 8x2 Side	36	0.48	7.38	0.46	0.46 @ 0 deg	0.46	0.42	0.72	0.77
Montney - Sliding Sleeve	Well 2	-	0	0	0.4	0	0.73	0.73	0.83	0.77
Permian	Well 1 – 100ft Side	62	15.44	14.11	0.43	0.286 @ 60 deg	0.72	0.73	0.78	0.93
Permian	Well 1 – 200ft Side	60	13.37	10.36	0.43	0.286 @ 60 deg	0.47	0.65	0.84	0.88
Permian	Well 1 – 250ft Top	19	9.82	17.25	0.43	0.26 @ 20 deg	0.55	0.66	0.81	0.84
Permian	Well 1 – 350ft Top	16	14.38	22.07	0.43	0.26 @ 16 deg	0.49	0.53	0.54	0.67
Permian	Well 1 – 350ft Side	45	8.39	14.04	0.43	0.27 @ 45 deg	0.51	0.52	0.66	0.69
Bakken	Well 1 - 18x1 Bottom	226	6.57	9.44	0.43	0.42 @ 226 deg	0.01	0.04	0.67	0.83
Bakken	Well 1 - 17x1 Side	262	10	9.44	0.43	0.41 @ 262 deg	0.02	0.15	0.61	0.77
Bakken	Well 1 - 16x2 Side	310	3.98	9.44	0.43	0.315 @ 310 deg	-0.27	-0.01	0.77	0.77

3.2.2 Divergence between different types of uniformity index

Uniformity index can be defined in a variety of different ways. It can be defined on a per-cluster basis or a per-shot basis, and it can be defined for proppant outflow, slurry outflow, or erosion. Downhole imaging is used to estimate the uniformity of erosion, and fiber optic is used to estimate the uniformity of slurry. There is not a measurement available that directly estimates proppant outflow itself. However, when analyzing simulation results, it is possible to calculate any of the three metrics. We usually focus on the per-cluster uniformity (rather than the per-shot uniformity), because this is probably more representative of the far-field fluid and proppant placement.

It is common to implicitly assume that the uniformity coefficient of erosion, slurry, and proppant are equal. However, our simulation results suggest that they can diverge considerably. Figure 12 shows cross plots of the slurry, proppant, and erosion uniformity index from the simulations calibrated to the 15 perforation designs in the study. The simulated erosion UI is systematically much lower than the simulated proppant or slurry UI. In the lowest cases, the erosion is near 0.0, while proppant and slurry UI remain greater than 0.6. The plots seem to suggest a linear relationship between these values, but the true relationship is likely nonlinear and multivariate. In some cases, UI of proppant, slurry, and erosion may be similar; in other cases, they may diverge considerably.
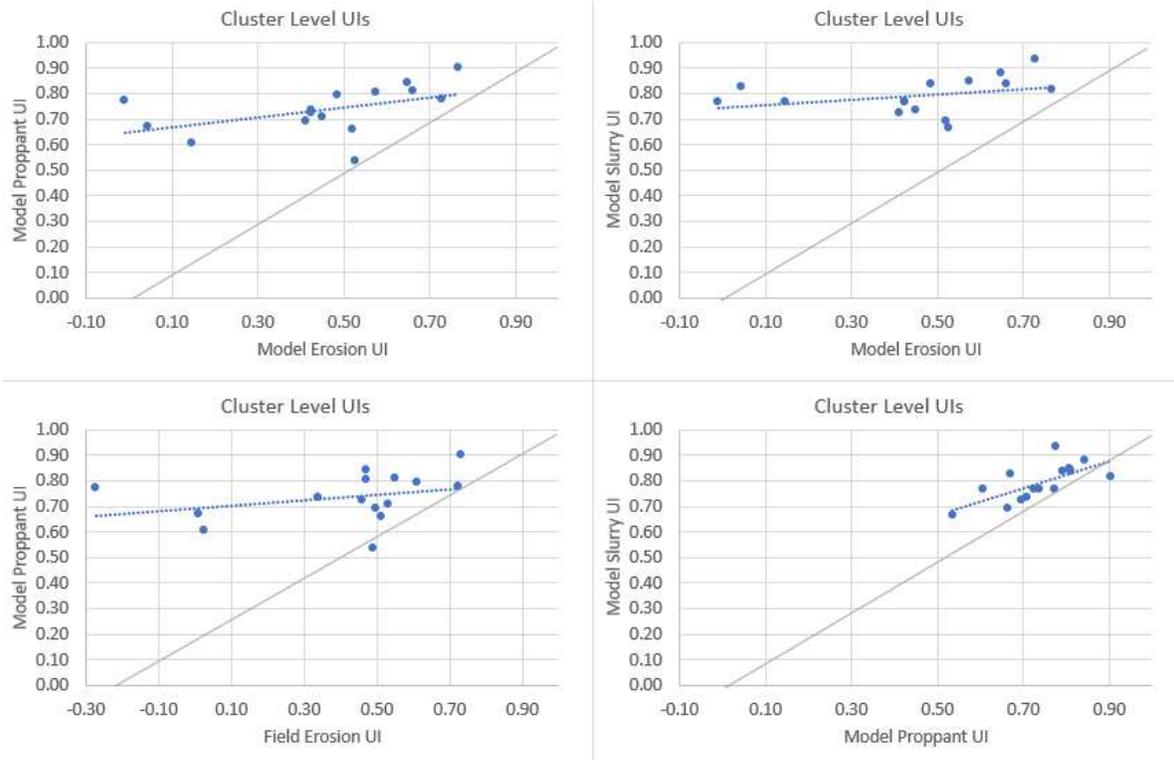
Figure 12: Cross-plots between cluster-level uniformity index of erosion, slurry, and proppant from the simulation matches to the three datasets.

The erosion-based uniformity index is highly dependent on the overall magnitude of erosion for a given well, which, naturally, is a function of the underlying base hole sizes assumed in the analysis. Error in the understanding of underlying base hole sizes, particularly in the phasing dependence of base hole size, can bias interpretation and systematically cause overestimated estimates of variability (i.e., underestimated values for uniformity index). In practice, the random variance in initial perforation diameter can be estimated by shooting 'dummy' perforation shots uphole of the final stage, and then never stimulating these holes. However, it is important to run these shots at a variety of phasing values in order to constrain the effect of phasing on initial diameter.

Figure 13 shows final perforation shot diameter versus phasing for the Bakken datasets discussed in Section 3.2.6. Based on check shots, the orange line shows our assumed estimate for the 'initial' diameter of each shot. However, because of random variance, there will be some shots that start with a lower initial diameter than the 'average.' When calculating the uniformity index for cluster-level erosion, we first calculate the difference between the total perforation area in a cluster post-completion and the initial perforation area based on the interpretation of the base hole size. We then calculate UI on these *area growth* values.
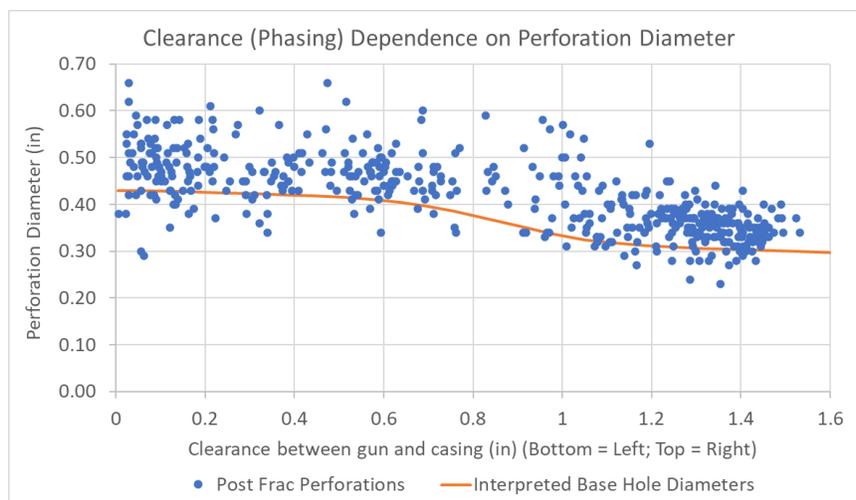
Figure 13: Final perforation diameter versus clearance from the Bakken dataset

Another potential source of apparent variability comes from the interpretation for initial hole diameter as a function of phasing. Unstimulated calibration shots performed at the heel of the well do not always sample all the phasings used along the lateral. For example, wells may have only 0° check shots, but include some stages with 90° phasing. In these cases, depending on the interpreter's assumption regarding the effect of phasing on initial hole size, this can impact the estimate for erosion and UI of erosion.

Finally, the erosion uniformity index is based on the perforation diameter profile after the full stage has been pumped. Slurry and proppant uniformity indices are the temporal integration of the instantaneous values of uniformity throughout the stage. Typically, uniformity is greatest at the beginning of the stage. As time progresses, uneven erosion degrades the uniformity of fluid outflow. The *instantaneous* slurry and proppant uniformity may have degraded significantly by the end of the stage, but consideration of the *cumulative* slurry and proppant uniformity will result in a significantly higher value of UI than the final *instantaneous* uniformity.

3.2.3 Montney P&P

3.2.3.1 Comparison between the Montney datasets

We analyzed two Montney plug and perf wells, referred to as MPP3 and MPP4.

Well MPP3 used 200 ft stage length with five clusters per stage and either three or four shots per cluster. The shots were oriented towards a 0˚ phasing, plus/minus 5.8˚ standard deviation on a 'per stage' basis, and plus/minus 6.1˚ standard deviation on a 'per shot' basis. The stages were stimulated with 40 bbl/ft of fluid and 3067 lbs/ft of 40/70 proppant. The target perforation diameter was 0.46 in. The actual perforation diameter at 0˚ was 0.46 in.

Figure 14 and Figure 15 show the actual and simulated erosion statistics for the MPP3 well. The data shows a strong inline effect, where proppant preferentially flows into the downstream shots in each cluster (Section 2.3). The overall perforation efficiency is high, with roughly 6% of perforations showing no erosion in the four shot designs and 1% showing no erosion in the three shot designs. The designs exhibit a slight toe bias, which is stronger in the three shot designs. The average uniformity index of cluster-level erosion is 0.61 in the three shot designs and 0.47 in the four shot designs. The simulated average cluster-level proppant uniformity index is 0.79 and 0.81 for the three and four shot designs respectively.

Well MPP4 used 315 ft stage length, eight clusters per stage, and either two or three shots per cluster. The clusters are inline within each shot. The phasing is fairly consistent within each stage but varies considerably, between stages. For purposes of assembling statistics, we have separated out the two and three shot designs into 'top' and 'side' oriented stages. The phasing variation is between plus/minus 0.48˚ and 19.2˚ on a 'per stage' basis, and plus/minus 7.38˚-11.01˚ on a 'per shot' basis.

The stages were stimulated with 30 bbl/ft of fluid and 3080 lbs/ft of 100 mesh proppant. The target perforation diameter was 0.46 in. In the simulations, there were no adjustments made for perf diameter as a function of clearance due to lack of calibration data and large gun OD relative to well.
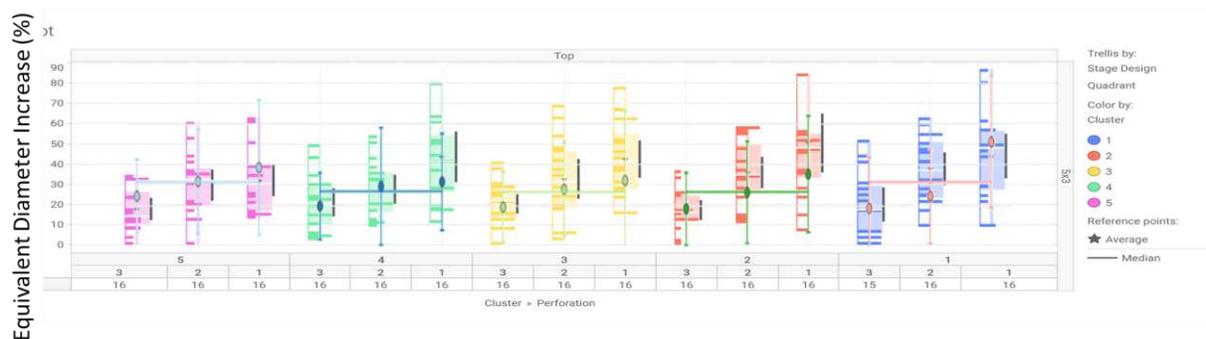
Figure 14: Actual and simulated perforation erosion by shot for the Montney 5x3 Top dataset. Flow is from left to right. The thick bars show the actual data, and the dots and thin bars show the simulated data.
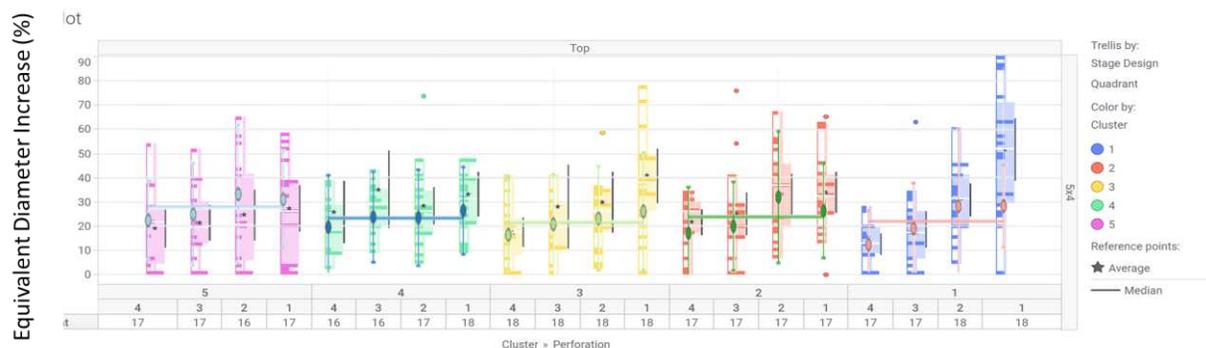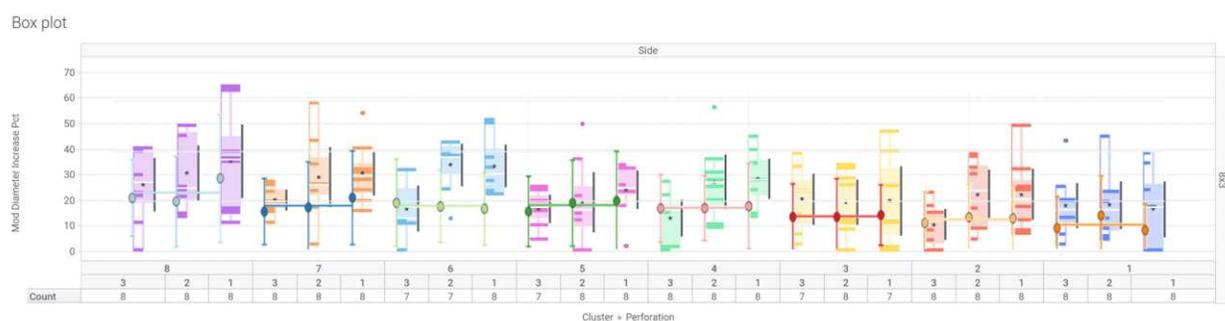

Figure 15: Actual and simulated perforation erosion by shot for the Montney 5x4 Top dataset. Flow is from left to right. The thick bars show the actual data, and the dots and thin bars show the simulated data.

Figure 16, Figure 17, Figure 18, and Figure 19 show the actual and simulated erosion statistics for the MPP4 well. As with the MPP3 well, the data exhibits a strong inline effect. Roughly 10% of perforation shots showed no indication of erosion. The three shot stages exhibit a mild heel bias in erosion; the two shot stages exhibit a mild 'U' bias, with the least erosion in the middle. The average uniformity index of cluster-level erosion is 0.52 in the three shot designs and 0.4 in the two shot designs. As noted in Table 4, the top orientations have a slightly lower erosion uniformity than the side orientations.
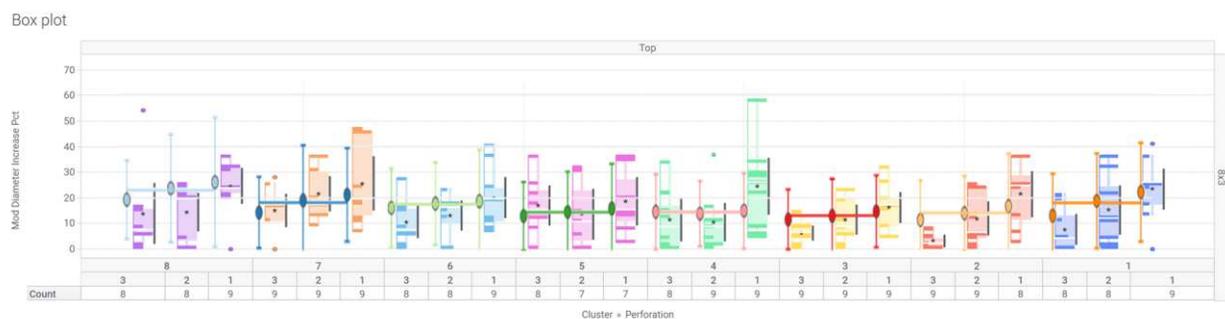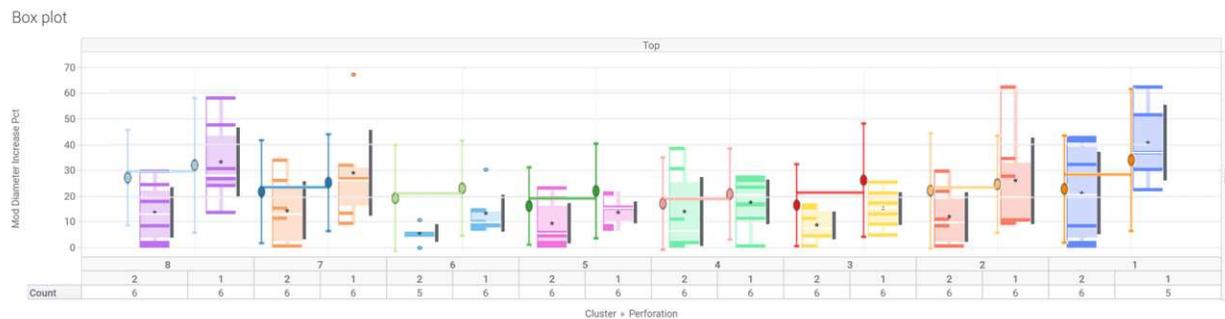
Figure 16: Actual and simulated perforation erosion by shot for the Montney 8x3 Top dataset. Flow is from left to right. The thick bars show the actual data, and the dots and thin bars show the simulated data.
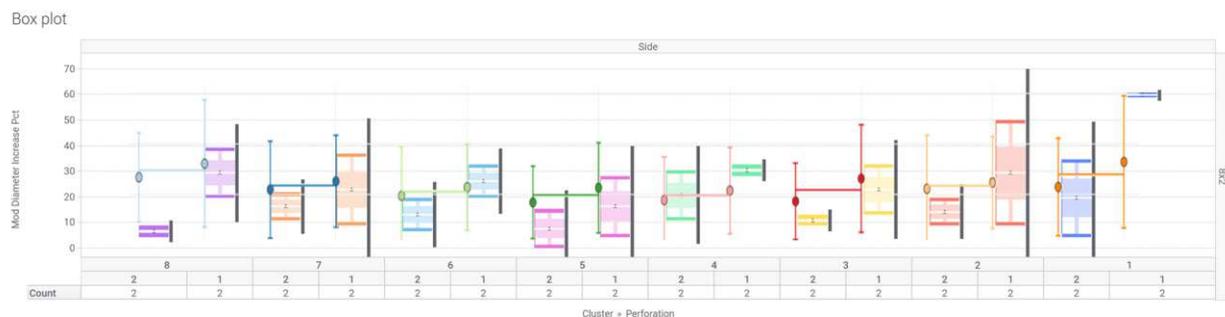

Figure 17: Actual and simulated perforation erosion by shot for the Montney 8x3 Side dataset. Flow is from left to right. The thick bars show the actual data, and the dots and thin bars show the simulated data.

The MPP3 and MPP4 wells have the proppant per cluster and similar fluid per cluster and surface injection rates. But they have different stage lengths, phasing, proppant type, and rate per cluster. In the model calibration match, parameters are mostly similar, except that the perforation erosion alpha parameter is significantly higher in MPP3 wells. The difference in alpha is probably due to the different types of proppant used. The suspension multiplier in the MPP3 wells is lower, but this is expected – it is a typical 'default' value to use a smaller suspension multiplier for the larger type of proppant, 40/70.

Compared to the stages with side phasing, the stages with top-side phasing have slightly less erosion along the middle of the stage and greater erosion at the heel. The simulation matches reproduce this observation. It occurs because gravitational settling causes less outflow from the clusters from the clusters in the middle of the stage. There must be more outflow at the final cluster to 'make up' for the reduced deficit from the clusters uphole.

Figure 18: Actual and simulated perforation erosion by shot for the Montney 8x2 Top dataset. Flow is from left to right. The thick bars show the actual data, and the dots and thin bars show the simulated data.

Figure 19: Actual and simulated perforation erosion by shot for the Montney 8x2 Side dataset. Flow is from left to right. The thick bars show the actual data, and the dots and thin bars show the simulated data.

3.2.3.2 Design optimization

Sensitivity analysis simulations were performed with the calibrated model to identify the perforation design that optimizes the cluster-level uniformity index of proppant outflow from the well.

With the MPP3 five cluster design, sensitivities were run varying the number of shots per cluster, while varying perforation diameter constant to maintain a constant 'designed' limited-entry of 2111 psi. Next, sensitivities were run varying phasing (using uniform shot phasing within the stage, in each case). The results are shown in Figure 20.
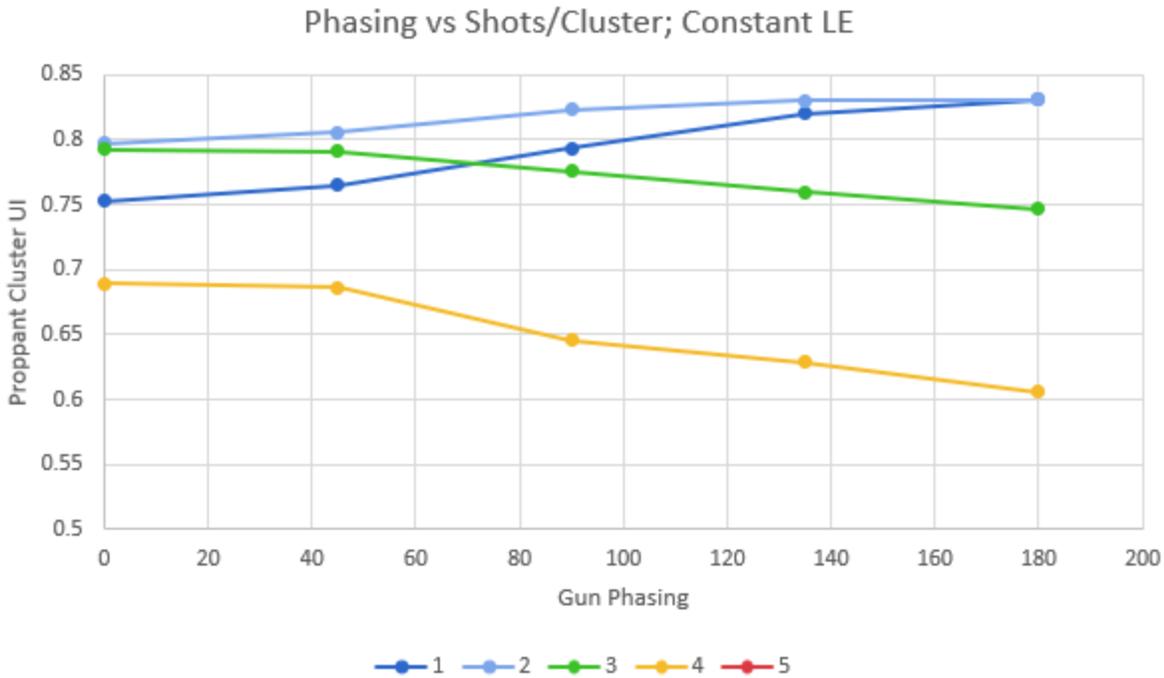
Figure 20: Sensitivity analysis simulations varying perforation strategy on the MPP3 well five cluster design.

With the three and four shot designs, the 0° phasing achieved the highest uniformity index, especially with the four shot design. Interestingly, with the one and two shots designs, the 0° designs performed slightly worse than shots oriented towards the side, or even the bottom, of the hole. With the three and four shot designs, the inline effect is so strong that there is a tendency for heel bias (Figure 21). Orienting the shots along the side or bottom of the hole make the heel bias even stronger, as gravitational settling encourages even more proppant outflow from the well before reaching the final cluster. With the one and two shot designs, the inline effect is weaker or nonexistent and there is not a heel bias (Figure 21). In this case, with 0° phasing, the is a very slight toe bias, which is reduced with 90° phasing.

Synthesizing these observations, we can see that 0° phasing tends to increase toe bias, while orienting perforations lower tends to reduce toe bias. Thus, if the erosion pattern is naturally tending towards heel bias, it can be beneficial to use 0° phasing to reduce that heel bias. Conversely, if the stage is naturally tending towards toe bias, then it may be beneficial to rotate the phasing around to the side, in order to mitigate the toe bias.

The highest performing design was two shots per cluster, with a target diameter and actual diameter varying from 0.56'' to 0.42'', depending on phase. With this design, the effect of phasing was only very slight. With this design, the average uniformity index could be increased from 0.79 to 0.83.
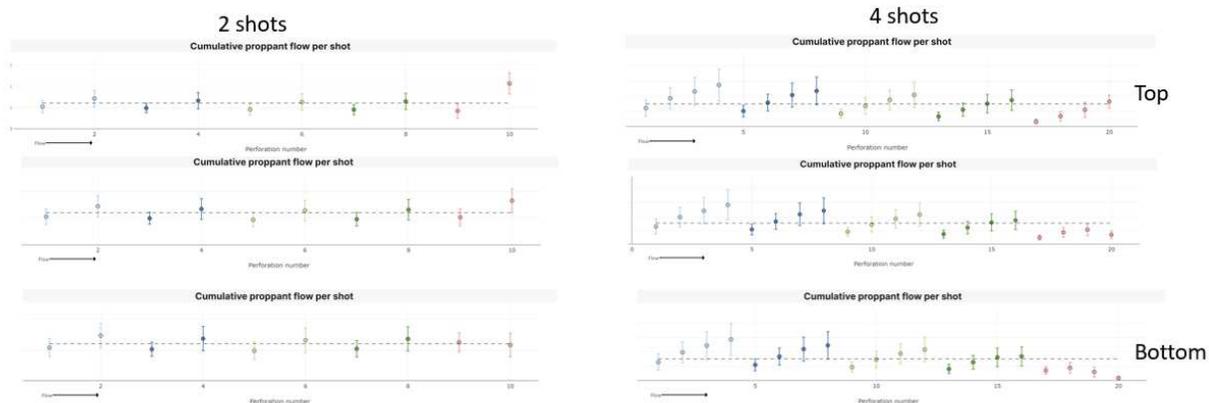
Figure 21: Comparison of sensitivities on two or four shots designs (0.56'' and 0.39'' designed diameter), with side, middle, and bottom phasing. Each dot shows the 'per-shot' results, and the whiskers show the P10/P90 ranges. The horizontal lines show the 'per-cluster' results. The shots in each cluster are plotted with separate colors. The horizontal dashed lines show the overall average.

The same sensitivity series was run for the MPP4 8 cluster design, as shown in Figure 22. In this case, however, UI is relatively insensitive to phasing. Despite the longer stage length which would often create more phasing dependence, MPP4 uses a much finer proppant than MPP3. With this finer mesh, gravitational settling is not as prominent, so phasing loses its importance. UI is maximized with 4/5 shots per cluster inline.
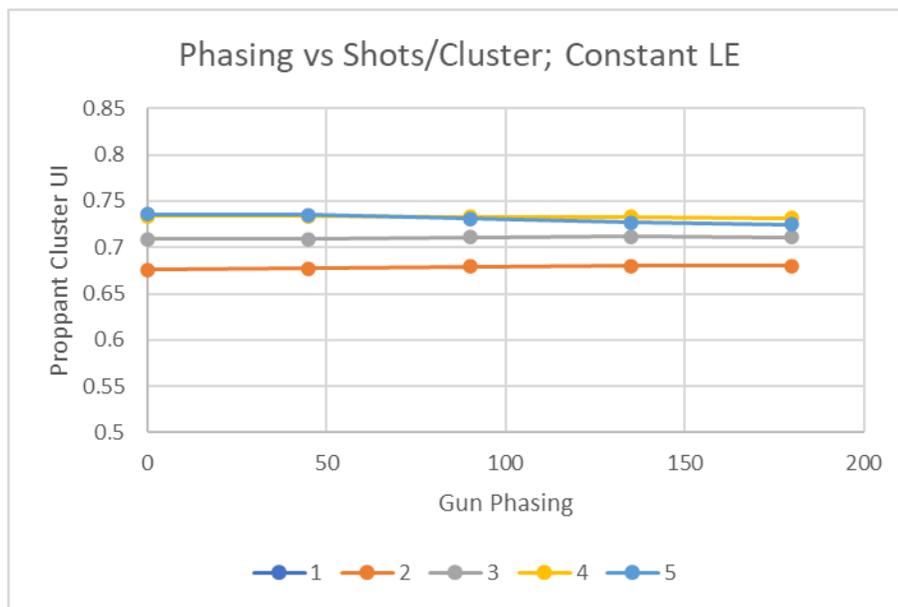
Figure 22: Sensitivity analysis simulations varying perforation strategy on the MPP4 well eight cluster design.

Finally, we performed an open-ended design optimization, varying different parameters to maximize UI. With the MPP3 five cluster well, proppant UI was increased to 0.834 with a design using 2 shots per cluster, 90° phasing, and initial diameter of 0.46''. This is a slight increase in the base LE by 300 psi. The erosion UI was predicted to be 0.474. The results are shown below in Figure 24.

For well MPP4 with 8 clusters, proppant UI was increased to 0.823 from the base case of 0.710. As shown in Figure 23, this design utilizes a tapered configuration with 3 shots at the heel-most cluster and 4 shots for the remainder of the stage. Limited entry is 2798 psi with a base perf diameter of 0.32''.

Flow distribution summary

| Name	Proppant per perf	Proppant per cluster	Slurry per perf	Slurry per cluster	Area change per perf	Uniformity index				Area change per cluster
Average	0.617	0.823	0.702	0.846	0.095					0.553
Median	0.640	0.839	0.724	0.859	0.199					0.590
STD	0.124	0.075	0.115	0.067	0.377					0.188

3 results
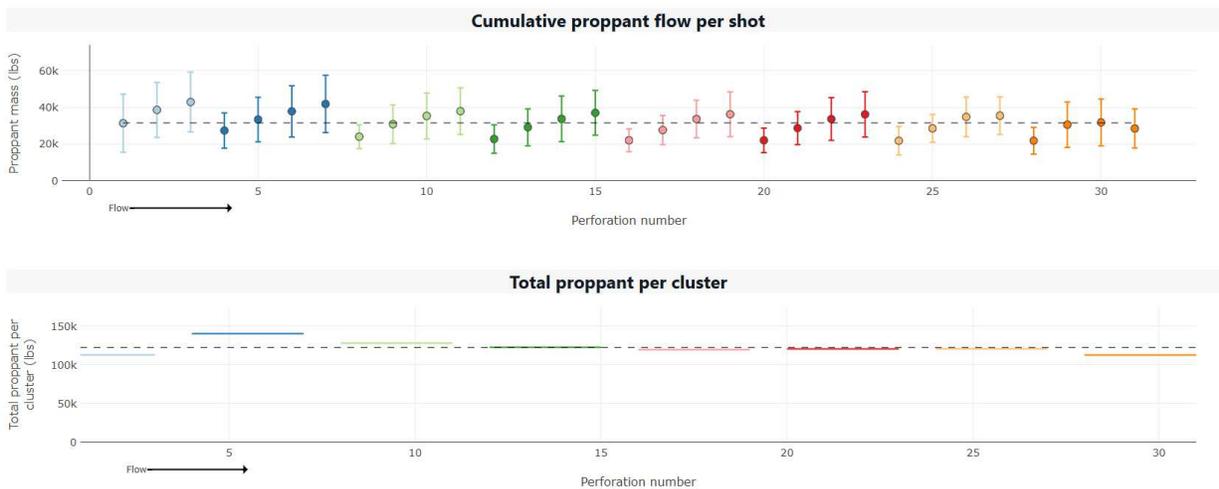
Figure 23: The optimal design for the MPP4 eight cluster well with 100M proppant. Each dot shows the 'per-shot' results, and the whiskers show the P10/P90 ranges. The horizontal lines show the 'per-cluster' results. The shots in each cluster are plotted with separate colors. The horizontal dashed lines show the overall average.

Flow distribution summary

Name	Proppant per perf	Proppant per cluster	Slurry per perf	Slurry per cluster	Area change per perf	Area change per cluster
			Uniformity index			
Average	0.684	0.834	0.794	0.865	0.198	0.474
Median	0.709	0.852	0.822	0.883	0.289	0.537
STD	0.106	0.087	0.100	0.075	0.366	0.267

3 results
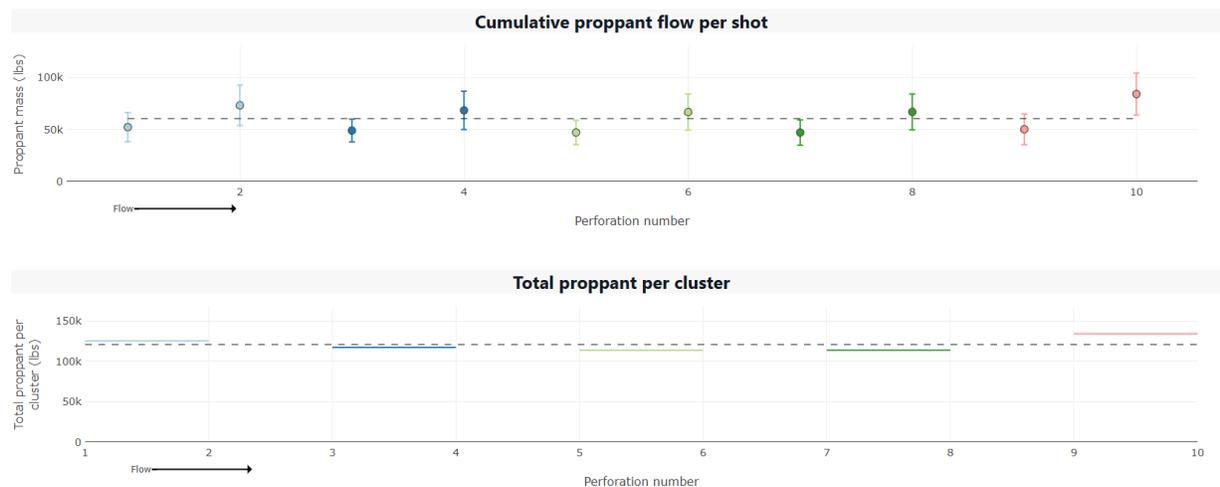
Figure 24: The optimal design for the MPP3 5 cluster well with a coarser proppant. Each dot shows the 'per-shot' results, and the whiskers show the P10/P90 ranges. The horizontal lines show the 'per-cluster' results. The shots in each cluster are plotted with separate colors. The horizontal dashed lines show the overall average.

3.2.4 Montney sliding sleeve

This well used a sliding sleeve design. At three locations along the stage, there were eight holes placed at 45 degree phasing. The holes were machined at the surface, prior to running the casing, and as a consequence, there was near-zero uncertainty in phasing or initial diameter. All eight holes were placed at exactly the same MD, unlike in a plug-and-perf, where there is a small MD offset from hole to hole.

All four stages exhibited strong heel bias, with the heel cluster eroding 52% more than the toe cluster on average. For all three clusters, perforations in the 1st quartile (top of the well) eroded the least; erosion was the strongest in the 2nd quartile (45 to 90 degree phasing) being 1.36x that of the first quartile perforations. Even so, the variance of erosion within a quartile of a cluster was wide with an average range of +/- 15%.

When history matching, a relatively high stress shadow of 500 psi combined with a gamma multiplier of 0.5 was required to match the level of heel bias shown in the data with only three clusters. Both of these parameters were higher than those used in all of the other plug-and-perf datasets in this project. With a 55 mesh proppant pumped, a suspension multiplier of 3.0 was used to be consistent with the other datasets.
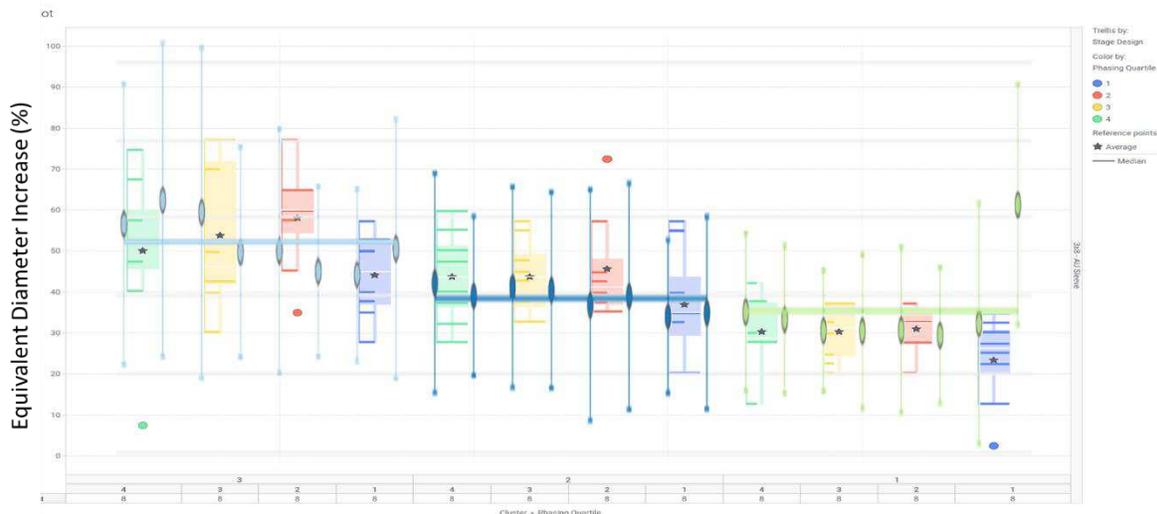
Figure 25: Actual and simulated perforation erosion by hole for the Montney Sliding Sleeve dataset. Flow is from left to right. The thick bars show the actual data, and the dots and thin bars show the simulated data.

Because of the limited sample size, the decision was made to remove spatial correlation from this model and treat the erosion variance for each individual perforation as independent. The nugget was set to 0.31 and the sill was set to 0. The average cluster-level erosion UI was 0.73. The model UI was 0.77, providing a good match. This choice was not necessarily needed to match the data; it would have alternatively been reasonable to set 'range' to a value more similar to that used in the other simulation matches.

Despite the perfectly uniform initial hole size and phasing, the data exhibited considerable random variance in erosion. Figure 26 shows the erosion for each shot in the four stages. This data is valuable because it demonstrates that variation in phasing and initial hole size – which inevitably occur in plug and perf completions – are not solely responsible for the observed variance in erosion. Even with perfectly uniform phasing and initial diameter, there is still a large amount of variability in erosion from stage to stage. The 'random' variability may be related to differences in local rock properties along the lateral, differences in the cement sheath, heterogeneities in the casing steel, or differences in loading along the casing, related to torque and drag.
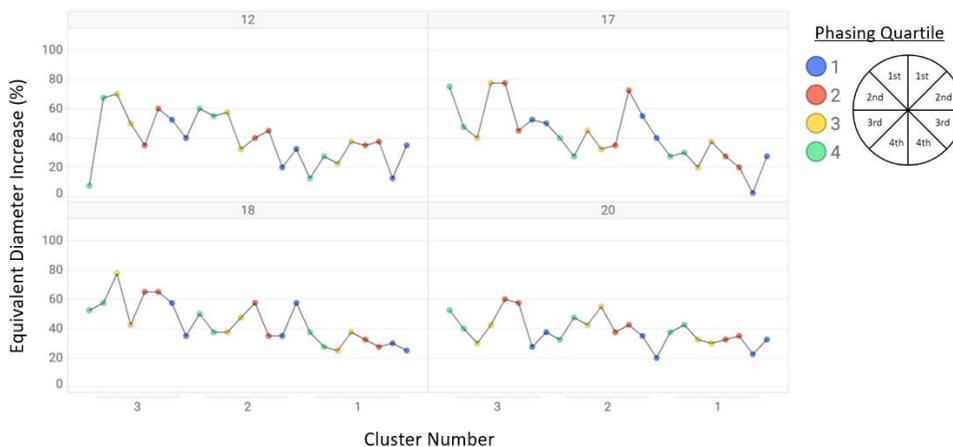

Figure 26: Measured percent increase in equivalent diameter by shot for four Montney sliding sleeve stages.

Shots in the upper quartile of the well eroded somewhat less than shots in other quartiles (Figure 28). This effect would be expected to weaken towards the toe, as the flow velocity drops and graviational effects strengthen. However, this trend was not evident in the data, probably because there were only three 'clusters' and so the velocity remained fairly high, even at the final cluster.
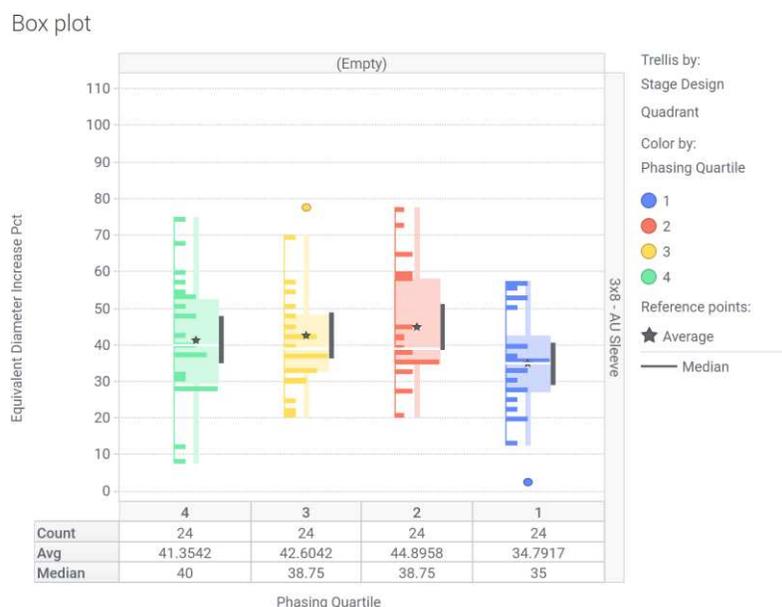

Figure 27: Diameter increase as a function of phasing for the Montney sliding sleeve stages.

In the StageOpt simulation, the 'final shot' showed an anomalously high erosion effect (Figure 25). This is due to a model limitation. The model assumes that each shot is placed immediately after the previous shot, by a few cm. But in the actual data, the shots were placed at precisely the same location. The result is a model artifact where there is a 'final' shot (in the model, though not in reality) that takes excess proppant.

3.2.5 Permian

In this dataset, we compare five designs – 100 ft stage with four clusters along the side, 200 ft stage with 8 clusters along the side, 250 ft stage with 10 clusters along the top, 350 ft stage with 14 clusters along the top, and 350 ft stage with 14 clusters along the side. In all cases, the perforations are inline, with mostly consistent orientation within the stage. The stages are usually tapered, with slightly more perforation shots towards the heel than the toe. Each design has similar fluid and proppant loading per cluster and per ft of lateral. The designed perforation pressure drop was similar in all cases, and perforation spacing was consistently 25 ft. The number of shots per cluster is varied, and so the fluid and proppant per shot is *not* constant. The designs with shorter stages have more shots per cluster, and correspondingly, less fluid and proppant per shot.

The data exhibits several key trends: (1) slight heel bias in the erosion profile for all but the longest stage length; (2) a "U" shaped erosion profile with the longest stage length; and (3) inline perforation effects with downstream perforations eroding more on average than the first perforation in a cluster.

All five scenarios were matched with a consistent set of model parameters, as shown in Table 3. The actual and simulated UI for the five scenarios are shown in Table 4. The designs with shorter stage length

tend to have greater uniformity. This is probably because there is less fluid and proppant outflow *per shot*. This causes less overall erosion and therefore, there is less time for nonuniformity to develop.
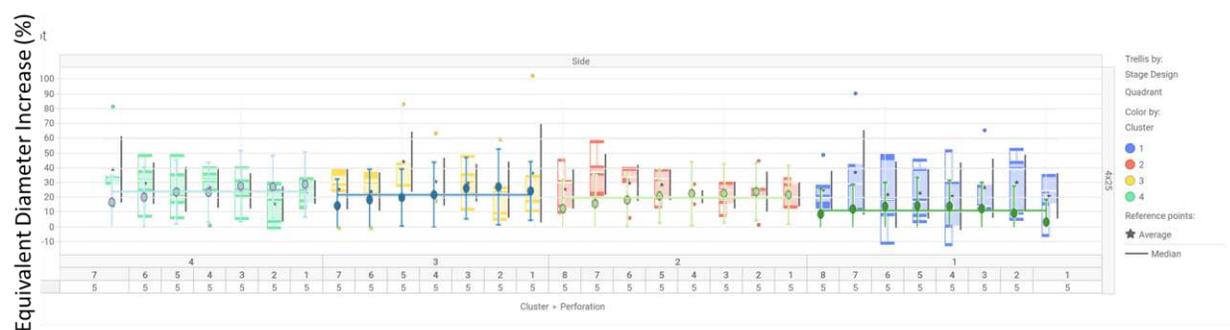

Figure 28: Actual and simulated perforation erosion by shot for the Permian 100 ft Side dataset. Flow is from left to right. The thick bars show the actual data, and the dots and thin bars show the simulated data.
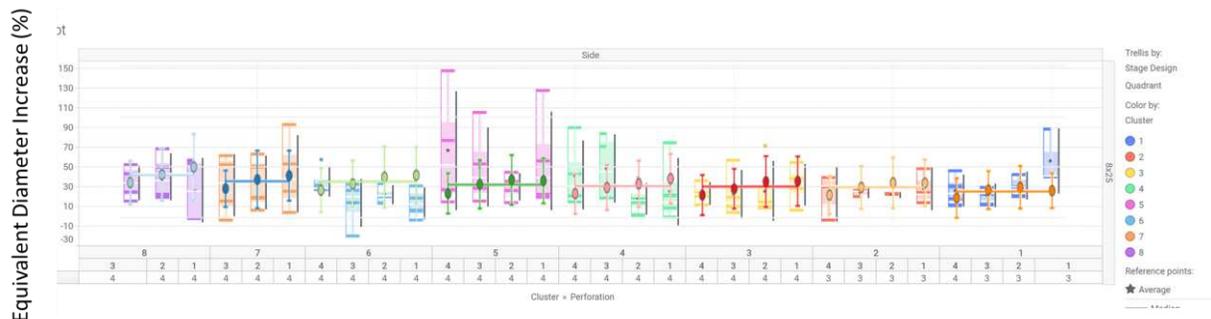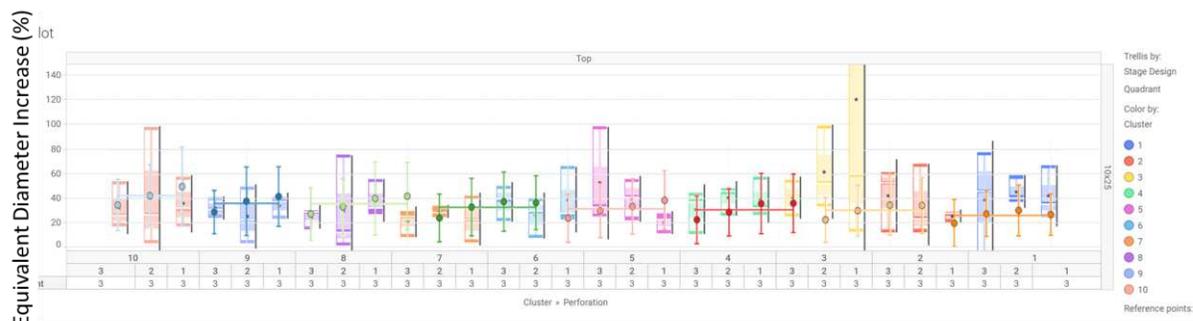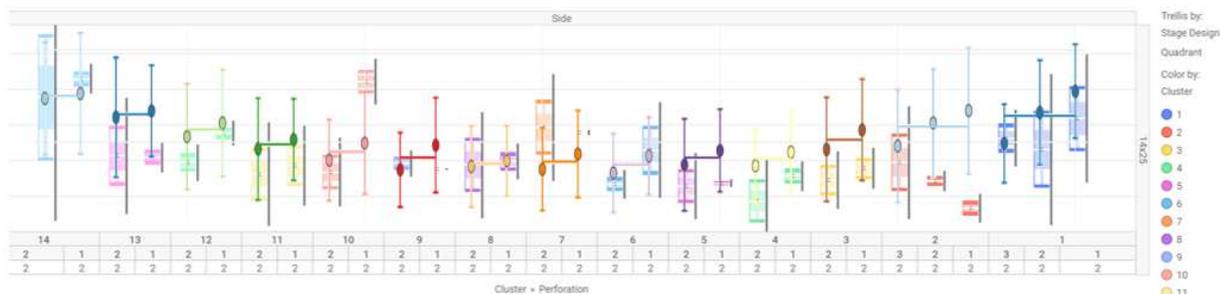
Figure 29: Actual and simulated perforation erosion by shot for the Permian 200 ft Side dataset. Flow is from left to right. The thick bars show the actual data, and the dots and thin bars show the simulated data.

Figure 30: Actual and simulated perforation erosion by shot for the Permian 250 ft Top dataset. Flow is from left to right. The thick bars show the actual data, and the dots and thin bars show the simulated data.
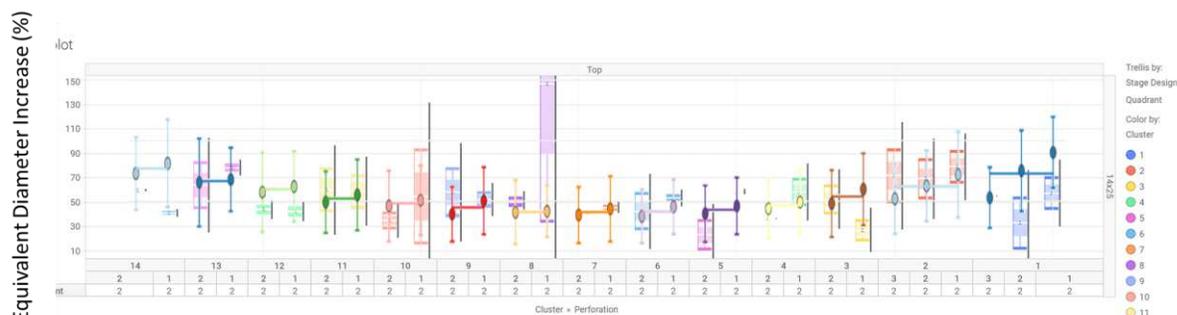

Figure 31: Actual and simulated perforation erosion by shot for the Permian 350 ft Top dataset. Flow is from left to right. The thick bars show the actual data, and the dots and thin bars show the simulated data.

Figure 32: Actual and simulated perforation erosion by shot for the Permian 350 ft Side dataset. Flow is from left to right. The thick bars show the actual data, and the dots and thin bars show the simulated data.

The 200 ft stage length model from this well was used to run sensitivities to explore alternative designs for optimization. Sensitivities were run exploring the phasing of the clusters (assuming perforations were inline within a cluster) as well as the number of shots per cluster. Initial perforation diameter was adjusted to maintain a constant limited entry pressure.

Figure 33 summarizes the results from the sensitivity analysis simulations. Figure 34 shows the proppant distribution per perforation, varying shots per cluster at a 90° phasing, while varying initial diameter to maintain constant designed limited-entry pressure. The designs with two and three shots per cluster perform best. Phasing has little effect. Figure 34 shows that with more shots per cluster, the inline effect strengthens, resulting in a deficit of proppant reaching the toe clusters. The design with three shots probably strikes the best balance.

Figure 33: The effect of shot count per cluster and phasing on cluster-level proppant UI.
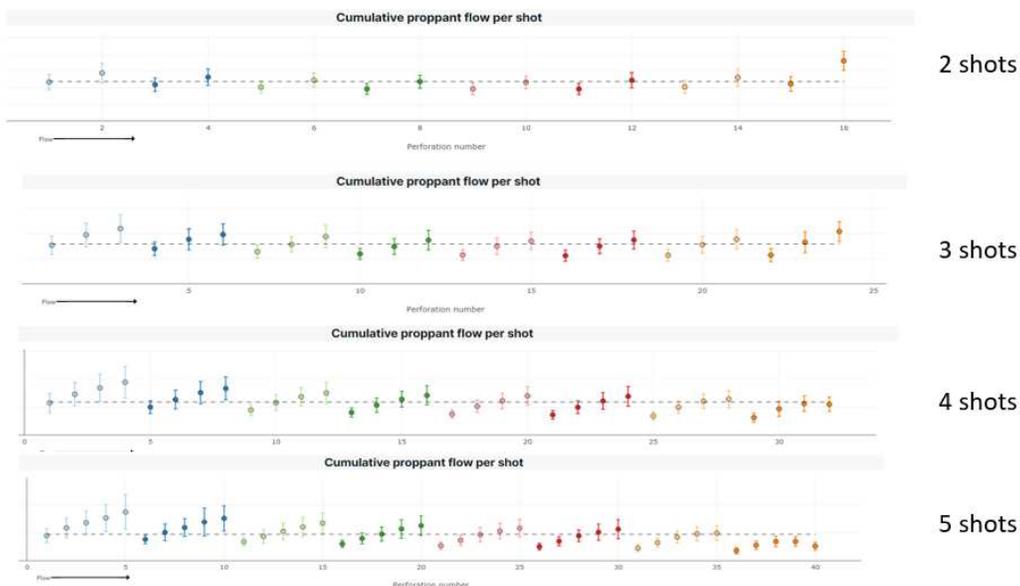
Figure 34: The distribution of proppant flow per shot as a function of shot count, with 90° phasing. The perforation diameter is varied to maintain constant limited-entry. Each dot shows the 'per-shot' results, and the whiskers show the P10/P90 ranges. The horizontal lines show the 'per-cluster' results. The shots in each cluster are plotted with separate colors. The horizontal dashed lines show the overall average.

Finally, we performed an open-ended design optimization, varying different parameters to maximize UI. With the 200 ft stage, proppant UI was increased to 0.872 with a design using 2 shots per cluster, 90° phasing, and initial diameter of 0.40''. The erosion UI was predicted to be 0.59.

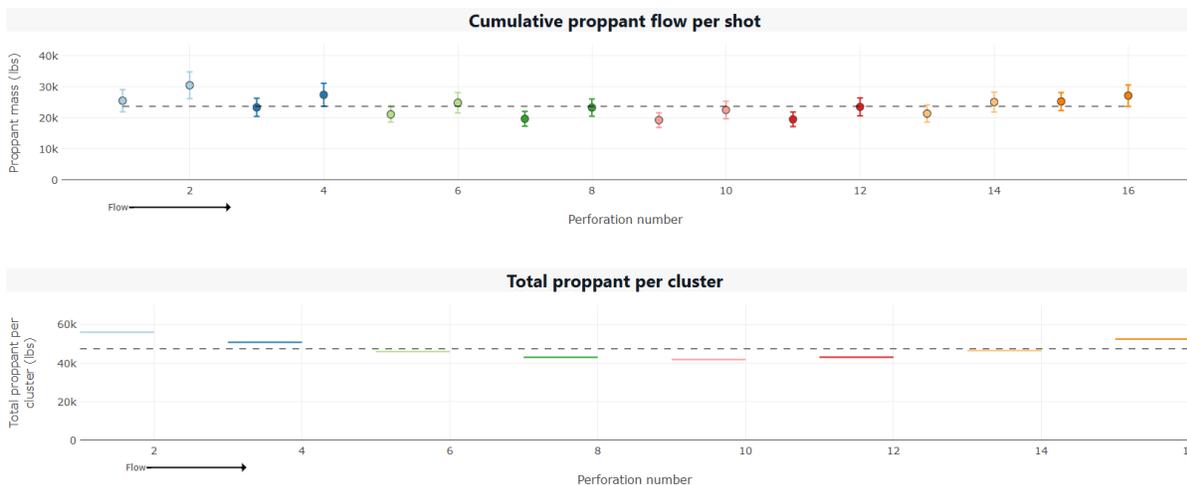| Name	Proppant per perf	Proppant per cluster	Slurry per perf	Slurry per cluster	Area change per perf	Area change per cluster
Average	0.823	0.872	0.839	0.862	0.449	0.593
Median	0.828	0.875	0.844	0.866	0.494	0.636
STD	0.037	0.035	0.035	0.034	0.210	0.164

3 results

Figure 35: The optimal design with the 200 ft stage length. The design perforation diameter is 0.40''. Each dot shows the 'per-shot' results, and the whiskers show the P10/P90 ranges. The horizontal lines show the 'per-cluster' results. The shots in each cluster are plotted with separate colors. The horizontal dashed lines show the overall average.

With the 350 ft stage, the optimal design was found to be heel/toe tapered scheme with shot count per stage - (2,2,2,2,3,3,3,3,3,3,3,3,2,2), and designed perforation diameter of 0.30''. The cluster-level proppant UI was improved to 0.81, from a starting point of 0.63.
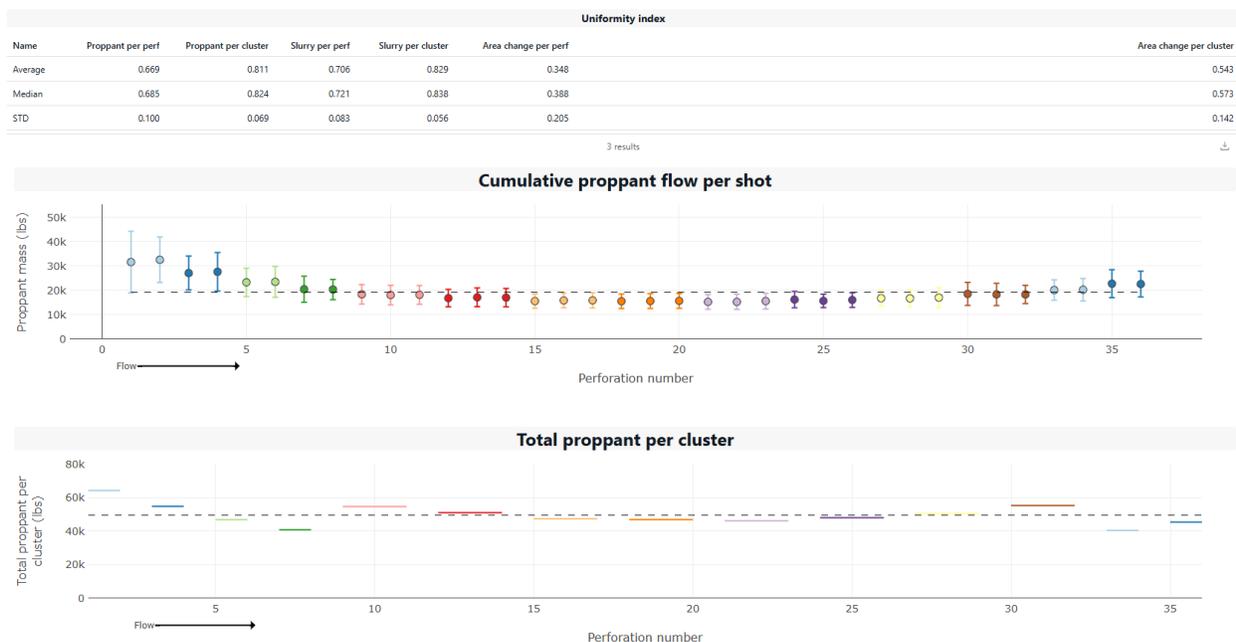
Uniformity index

Name	Proppant per perf	Proppant per cluster	Slurry per perf	Slurry per cluster	Area change per perf	Area change per cluster
Average	0.669	0.811	0.706	0.829	0.348	0.543
Median	0.685	0.824	0.721	0.838	0.388	0.573
STD	0.100	0.069	0.083	0.056	0.205	0.142

3 results

Figure 36: The optimal design with the 350 ft stage length. The design perforation diameter is 0.30''. Each dot shows the 'per-shot' results, and the whiskers show the P10/P90 ranges. The horizontal lines show the 'per-cluster' results. The shots in each cluster are plotted with separate colors. The horizontal dashed lines show the overall average.

3.2.6 Bakken

3.2.6.1 Comparison between the Bakken Designs

In this dataset, stages varied in length, with uniform cluster spacing and 15-20 clusters per stage. Stages used either one or two shots per cluster. A permanent fiber was cemented behind casing in the well. The fiber gradually coils around the casing, and so from stage-to-stage, the perforation orientation was gradually rotated in order to perforate in the direction away from the fiber. There were three stage designs with sufficient frequency to provide adequate sample size for analysis – 18x1 (bottom phasing), 17x1 (side phasing), and 16x2 (side phasing). There were not enough stages with top-side phasing for analysis. The cluster spacing was 18 ft. All perforations are inline.

To illustrate the degree of random variance from stage to stage, Figure 37 shows erosion for each shot in the seven stages with side-oriented shots, 16 clusters per stage, and 2 shots per cluster. The stages exhibit high variability from cluster to cluster, a modest tendency for spatial correlation in erosion from one cluster to the next, and a variety of different 'trends' (heel bias, toe bias, or neutral bias).
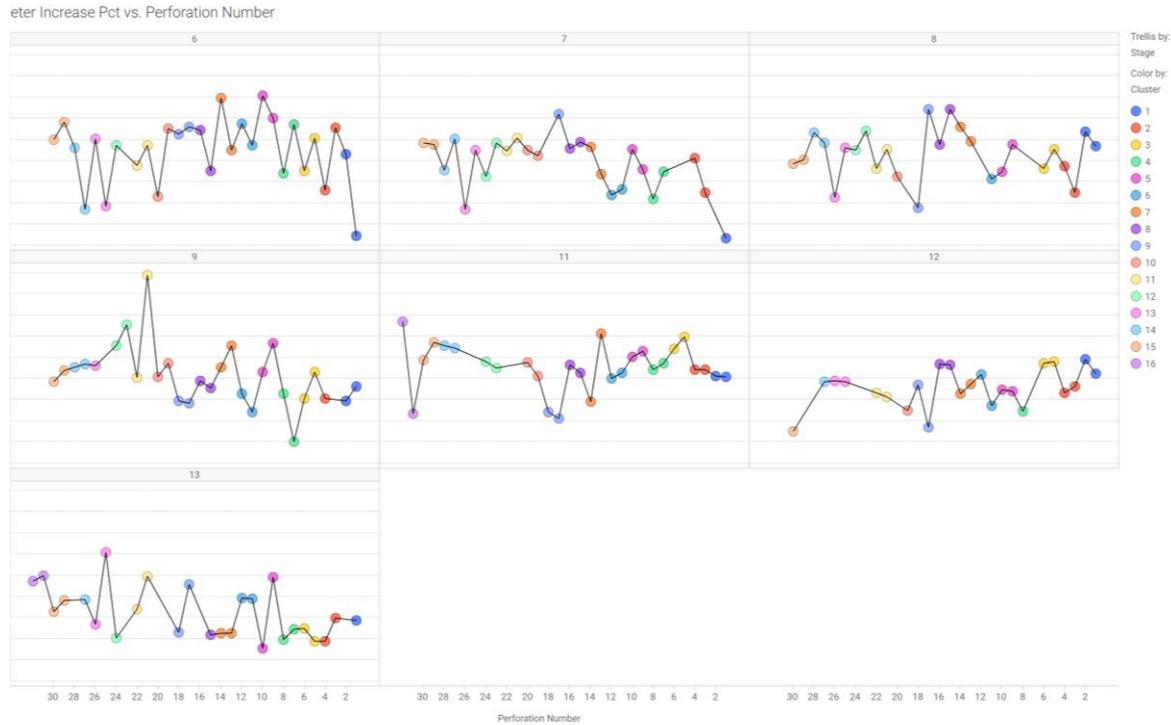
Figure 37: Examples of erosion by perforation number for the designs with 16 clusters, 2 shots per cluster, and side-oriented shots.

Figure 38, Figure 39, and Figure 40 show the statistically aggregated model and actual results from the 16x2 side, 17x1 side, and 18x1 bottom designs. In particular, Figure 40 shows the statistical aggregation of the data from Figure 37. The 16x2 design exhibits a modest heel bias, while the 17x1 and 18x1 designs exhibit a more neutral or ambiguous bias trend. This difference was also predicted by the model. In the design with two shots per cluster, the inline effect weakens the effect of inertia by enabling proppant that 'misses' the first shot to enter the second shot. Thus, adding the second shot causes more tendency towards heel bias.
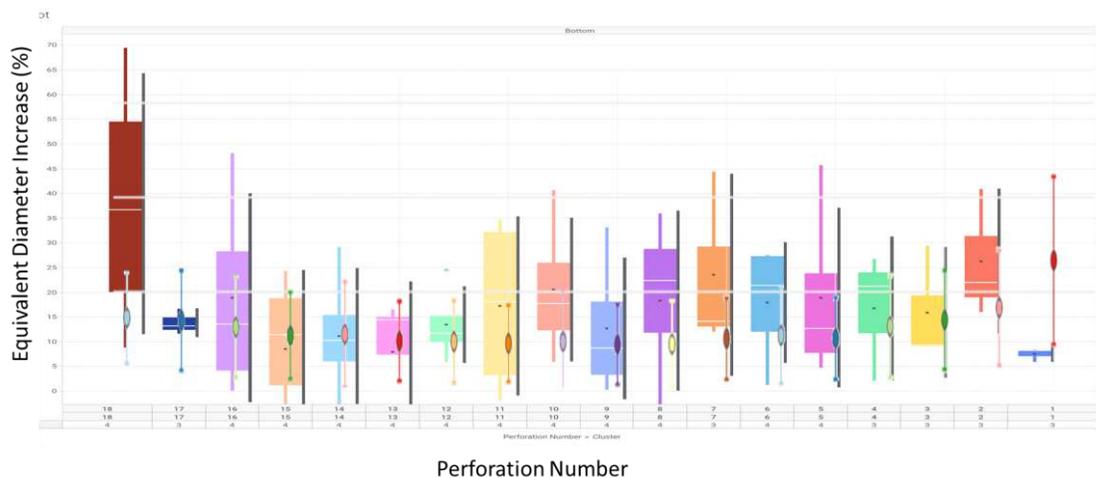
Figure 38: Actual and simulated perforation erosion by shot for the Bakken 18x1 Bottom dataset. Flow is from left to right. The thick bars show the actual data, and the dots and thin bars show the simulated data.
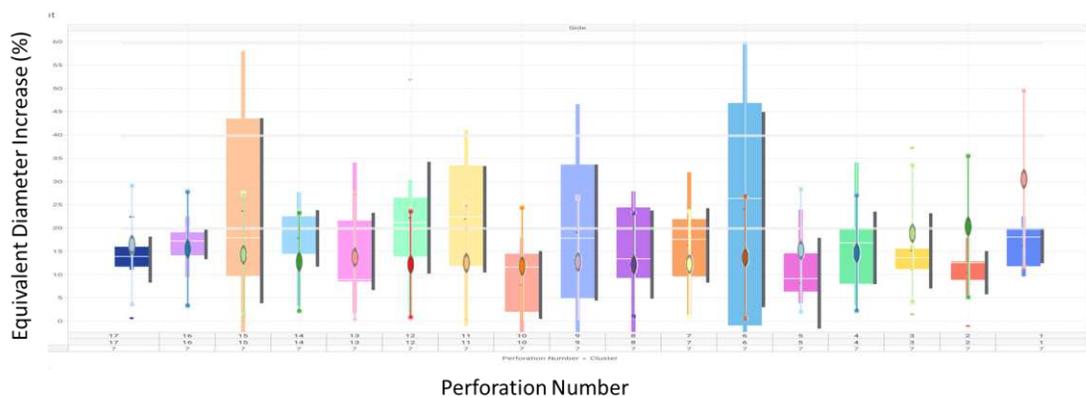

Figure 39: Actual and simulated perforation erosion by shot for the Bakken 17x1 Side dataset. Flow is from left to right. The thick bars show the actual data, and the dots and thin bars show the simulated data.
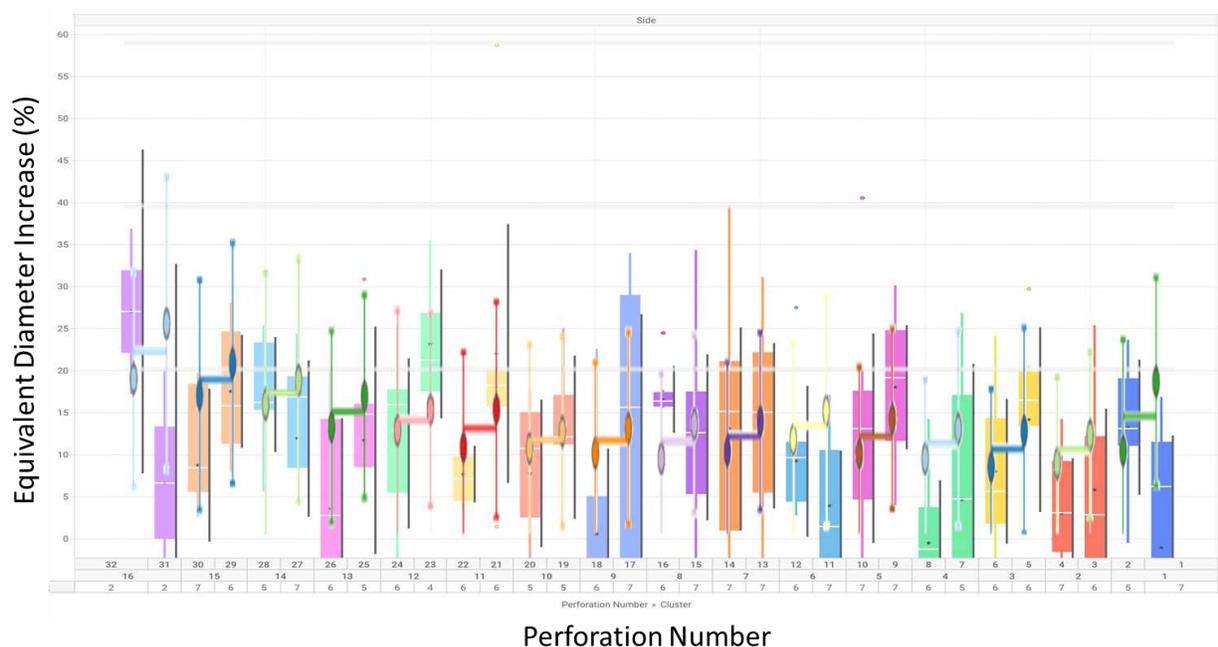
Figure 40: Actual and simulated perforation erosion by shot for the Bakken 16x2 Side dataset. Flow is from left to right. The thick bars show the actual data, and the dots and thin bars show the simulated data.

As noted in Section 3.2.2, the simulation results consistently predict lower uniformity index for erosion than for slurry or proppant outflow. In this Bakken dataset, we had a unique opportunity to test that result because cemented fiber was available to provide uniformity index estimates for slurry, while imaging was performed to provide uniformity index estimates for erosion. As predicted by the simulations, the slurry uniformity index was much higher – 0.82, 0.81, and 0.87 for the 16x2, 17x1, and 18x1 designs, respectively, while the observed erosion uniformity index was between (-0.27) and 0.02 for the three designs. The simulated proppant and slurry UI – which are consistent with the fiber-measured slurry UI – suggest that the actual uniformity of outflow during these stages was 0.77-0.83, relatively similar to the other designs compared during the study.

The erosion UI was particularly low in this Bakken dataset, compared with the other datasets. Counter-intuitively, this occurred because of the relatively low amount of overall erosion occurring in this dataset. The proppant per cluster was 80% to 50% smaller than that of the other data sets. With a smaller amount of erosion, the effect of random variability in 'initial diameter' has a stronger effect on the 'estimated' erosion UI, which causes the measured erosion UI to be especially low relative to the actual proppant outflow UI.

3.2.6.2 Bakken Design Optimization

For this well, sensitivities were run on the 17x1 model to explore optimization. Figure 41 shows the results from sensitivities on phasing and shots per cluster. Assuming constant limited entry, a greater number of shots/cluster (2-3) increased proppant uniformity in comparison to the 1 shot per cluster base case. Additionally, phasing at the side of the well was optimal compared to a top orientation; a side phasing appears to counteract inertial effects that were creating a toe bias by taking advantage of gravitational settling.
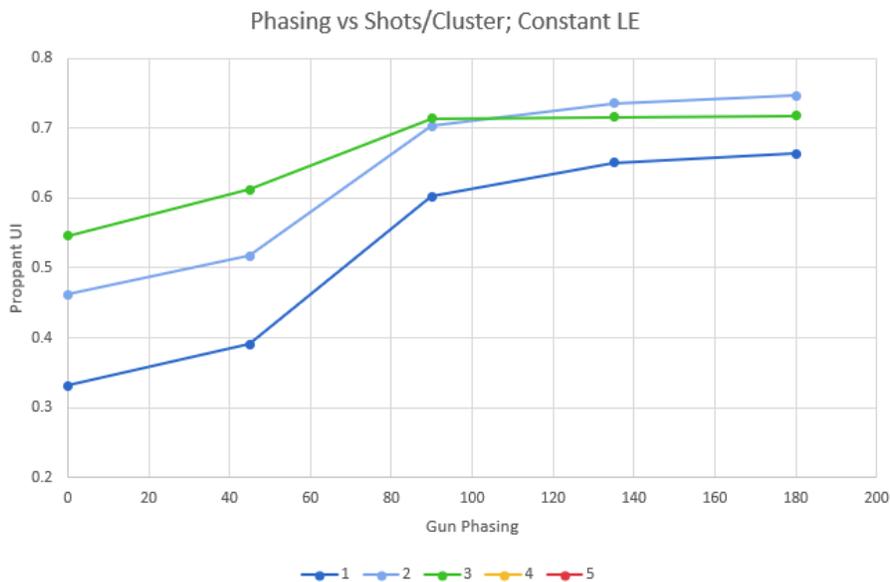
Figure 41: Cluster-level uniformity index of proppant outflow, as a function of phasing and shots per cluster. Perforation diameter is varied with shots per cluster in order to maintain constant designed perforation pressure drop.

For the open-ended optimization, we achieved a design that had a proppant per cluster UI of 0.798 compared to 0.607 base for a 17 cluster design, a 32% improvement. This was achieved with a phasing of 135°, 2 shots per cluster, and reducing the limited entry to 1200 psi. This design was best at offsetting the impacts of the long stage length – greater stress shadowing and gravitational settling.
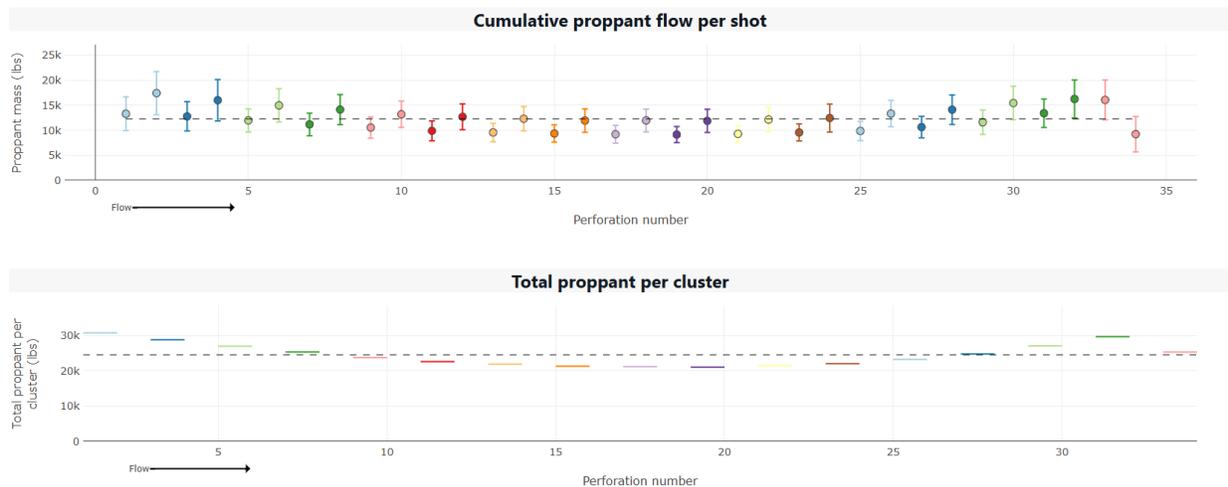

Figure 42: The optimal design with 17 clusters. The design perforation diameter is 0.38''. Each dot shows the 'per-shot' results, and the whiskers show the P10/P90 ranges. The horizontal lines show the 'per-cluster' results. The shots in each cluster are plotted with separate colors. The horizontal dashed lines show the overall average.

3.2.7 Compare/contrast between datasets

The distribution of slurry flow, proppant flow, and erosion depends on the interaction of processes with differing effects – stress shadowing, inertia, gravity, inline effects, perforation pressure drop, erosion, and more. Depending on the relative magnitude of these effects, stages may exhibit a diversity of trends – heel bias, toe bias, heel/toe bias, etc. The stage design has a major effect on these behaviors – stage length, shots per cluster, perforation diameter, perforation phasing, etc. Also, the trends appear to be determined – in part – by physical parameters related to local conditions such as steel and cement quality, proppant source, stress state, rock properties, etc.

Because of this variability, it is not possible to generalize and say that a certain phasing or cluster design is always the 'best' design. It is always advisable to use downhole imaging to provide calibration data. Once a model is calibrated to site-specific data, it is possible to run what-if scenarios to evaluate alternative designs for future wells.

Every dataset that had inline perforations showed increased relative erosion for the downstream perforations in a cluster. Therefore, we can conclude that if we want to reduce toe-side flow, we can choose to use inline perforation.

Longer stages (with cluster spacing held constant) showed a more "U"-shaped erosion profile with greater allocations to the heel and toe of the stage. This understimulation of the middle of the stage generally resulted in lower uniformity. As discussed in Section 3.2.5, heel/toe tapering may be a successful strategy to mitigate heel/toe bias.

Shots phased near the top of the well tend to be affected by gravitational settling, resulting in greater fluid/proppant flow in the final cluster. This effect is weaker with smaller diameter proppant. Considering this effect, there is not a single uniform recommendation on which phasing is best for uniformity. Recommended changes depend on whether the stage already exhibits heel or toe bias.

With regards to history matching and numerical fitting parameters, most parameters were fairly consistent across the datasets: (a) inline correction multiplier of 3.0, (b) suspension multipliers of 3x and 10x for 40/70 mesh and 100 mesh, respectively, (c) erosion gamma multiplier from 0-0.2, (d) fracture net pressure from 100-200 psi.

For parameters that were varied individually between datasets, and were *not* observed to be mostly consistent, we identified three: (a) erosion alpha, (b) fracture net pressure, and (c) stress shadow from the previous stage. Of these, the erosion alpha exhibited the greatest influence and was the most variable from case to case. It is affected by a variety of factors that are not directly considered by the model – proppant angularity, casing grade and quality, cement sheath quality, torque/drag on the casing that leads to locked-in strain, and/or other unknown effects.

The stage-by-stage data exhibits significant variability. Therefore, for calibration, it is important to use imaging to measure erosion on many stages (ideally more than 10-20) with identical design, in order to achieve a statistically significant sample.

3.2.8. Sensitivity analysis simulations on the effect of perforation consistency

Figure 43 shows a tornado plot indicating the relative change in the proppant UI when varying perf diameter uncertainty from 0 to 0.05'', cluster phasing uncertainty from 0 to 60 degrees, and perf phasing uncertainty from 0 to 60 degrees. This sensitivity was run on the optimized design from the 350 ft Permian dataset. The 'cluster-level' variance refers to differences from one cluster to the next (but is the same for all shots in each cluster); the 'perf-level' uncertainty refers to variability from shot-to-shot. Reducing cluster-level phasing variance was the most important factor that influenced overall uniformity

for the given design. Perforation diameter variance was the second most impactful parameter. Individual perf phasing uncertainty was the least impactful parameter, with a +/- 2% effect on UI.

In this case, exploring gun or charge options with more consistent exit-hole sizes as well as high quality gun orienting solutions may both improve UI substantially. Other cases may show a benefit in reducing variance in one design parameter or another.
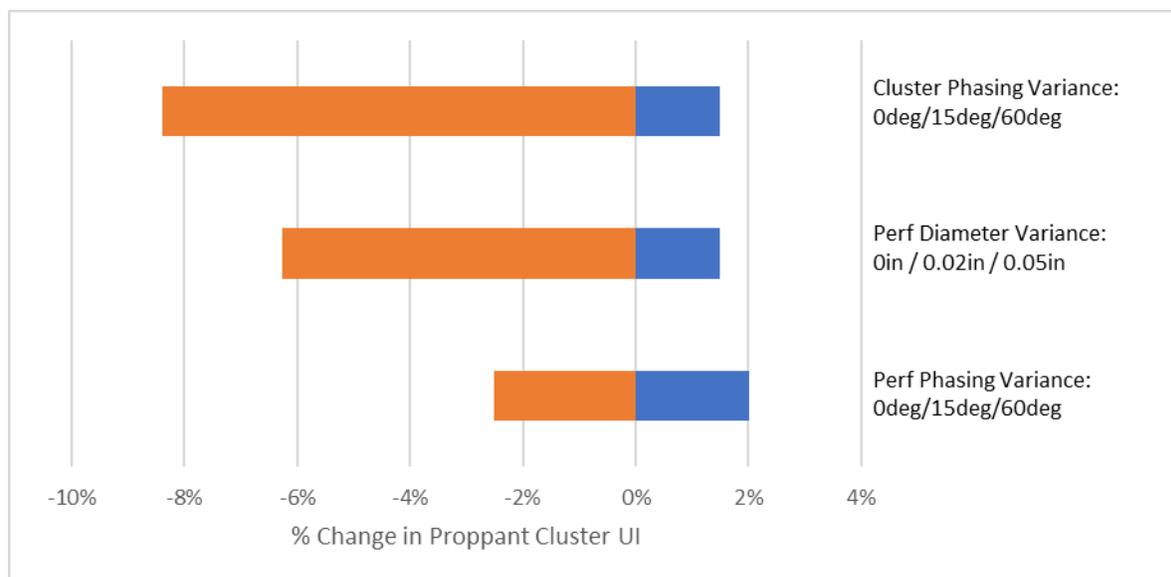

Figure 43: Sensitivity analysis simulations on the effect of random variance in initial shot diameter, cluster-by-cluster phasing uncertainty, and shot-by-shot phasing uncertainty.

4. Conclusions

In recent years, downhole imaging technologies have delivered an explosion of data on perforation erosion. At the same time, the technical community has invested in research to better-characterize the processes that drive proppant transport and outflow from the well. In this study, we combine insights from the literature into a single integrated simulator and compare the simulation results with a diverse collection of field datasets. Based on this comparison, we propose several improvements to the original simulation approach, improving its handling of inline perforating, proppant suspension, and random variance.

The simulator has a variety of 'tuning' parameters. However, comparison with field data suggests that most parameters can be set to a single, consistent value. Modification of a smaller subset of parameters is sufficient for calibration to field data.

The simulator predicts that measurements of erosion UI (uniformity index) cannot be assumed equivalent to proppant-outflow or slurry-outflow UI. The erosion uniformity will tend to be lower. This model prediction is supported by a dataset in our study where fiber-derived values of slurry uniformity were observed to be substantially higher than imaging-derived estimates of erosion uniformity. The simulation match suggests that both measurements were correct – the slurry uniformity truly was greater than the erosion uniformity.

Stage-to-stage variability in erosion profile is substantial. It is essential to collect data from enough stages to achieve statistical significance.

For each calibrated dataset, we performed sensitivity analysis on phasing and shots per cluster to assess their impact on uniformity. We also performed an open-ended optimization of design to find the best

possible value of UI. Across the datasets, the optimized designs improved cluster-level proppant-outflow UI by 0.12-0.19. According to the study from Cipolla et al. (2024), this implies a production uplift of 3-4.75%. While incremental, this is an impressive improvement, considering that these changes to perforation design can be made at little or no additional cost.

As noted by Dontsov et al. (2024), maximizing perforation pressure drop is not always optimal, because very high perforation pressure drop can lead to large, uneven erosion that degrades uniformity over time. To mitigate inertial effects and take advantage of the inline effect, the results suggest that it is sometimes advantageous to use a larger number of smaller-diameter, inline shots per cluster, rather than a smaller number of relatively larger shots per cluster.

There is no single uniform recommendation for the 'best perforation design.' Depending on stage architecture, pump schedule, and local geologic factors, stages may tend towards heel bias, toe bias, heel/toe bias, or a neutral bias. Depending on which type of bias is present, the design that maximizes uniformity will vary. In some cases, 0° phasing performs best; in others, 90° inline perforating performs best; in some cases, phasing has only a modest effect. In some wells, especially with longer stages, customized taper designs with variable shots per cluster may be beneficial. In other cases, uniform shots per stage are sufficient.

Overall, integrating physical insight with high-quality field diagnostics unlocks opportunities to make low-cost improvements to perforation design and maximize well performance.

References

Ahmad, F.A., and Miskimins, J.L. 2019a. Proppant transport and behavior in horizontal wellbores using low viscosity fluids. In Proceedings of the Hydraulic Fracturing Technology Conference and Exhibition, Houston, TX, SPE-194379-MS.

Ahmad, F.A. and Miskimins, J.L. 2019b. An experimental investigation of proppant transport in high loading friction-reduced systems utilizing a horizontal wellbore apparatus. In Proceedings of the Unconventional Resources Technology Conference, Denver, CO, URTEC-2019-414-MS.

Ahmad, F. 2020. Experimental investigation of proppant transport and behavior in horizontal wellbores using low viscosity fluids. PhD thesis, Colorado School of Mines, 2020.

Ahmad, F.A., Miskimins, J.L., Liu, X., Singh, A., and Wang, J. 2021. Experimental investigation of proppant placement in multiple perforation clusters for horizontal fracturing applications. In Proceedings of the Unconventional Resources Technology Conference, Houston, TX, URTEC-2021-5298-MS.

Bell, W.T., R.A. Sukup, and S.M. Taruq. 1987. Perforating. SPE Monograph Series, Vol. 16..

Cipolla, Craig, Ankush Singh, Mark McClure, Michael McKimmy, and John Lassek. 2024. The perfect frac stages – What's the value? In Proceedings of the Unconventional Resources Technology Conference, Denver, CO, URTEC-4044071.

Cramer, D.D. 1987. The Application of Limited-Entry Techniques in Massive Hydraulic Fracturing Treatments. In Proceedings of the SPE Production Operations Symposium, Oklahoma City, OK, SPE-16189-MS.

Cramer, D., Friehauf, K., Roberts, G., and Whittaker, J. 2020. Integrating distributed acoustic sensing, treatment-pressure analysis, and video-based perforation imaging to evaluate limited-entry-treatment effectiveness. SPE Prod & Oper, 35:0730–0755, SPE-194334–PA.

Cramer, David, and Kyle Friehauf. Methods for Assessing Proppant Coverage Along the Lateral for Plug-And-Perf Treatments. In Proceedings of the Hydraulic Fracturing Technology Conference and Exhibition, Houston, TX, SPE-217778-MS.

Dhuldhoya, Karan, and Kyle Friehauf. 2022. Applications of distributed strain sensing via Rayleigh frequency shift: Illuminating near-well and far-field fracture characteristics. In Proceedings of the Unconventional Resources Technology Conference, Houston, TX, URTeC-3721749.

Dontsov, E.V. 2023. A model for proppant dynamics in a perforated wellbore. Int. J. Multiph. Flow, 167:104552.

Gillies, R.G. 1993. Pipeline flow of coarse particle slurries. PhD thesis, University of Saskatchewan.

Gruesbeck, C. and Collins, R. E. 1982. Particle transport through perforations. Society of Petroleum Engineers Journal, 22(06):857–865.

Kaufman, Peter, Mark McClure, Nick Franciose, Sean Owens, Fabiano Srur, and David Russell. Optimizing completions in tank style development. 2019. In Proceedings of the Unconventional Resources Technology Conference, Denver, CO, URTeC-2019-608.

Lecampion, B., J. Desroches, X. Weng, J. Burghardt, and J. E. Brown. 2015. Can we engineer better multistage horizontal completions? Evidence of the importance of near-wellbore fracture geometry from theory, lab and field experiments. In Proceedings of the SPE Hydraulic Fracturing Technology Conference and Exhibition, The Woodlands, TX, SPE-173363-MS.

Liu, X., Wang, J., Singh, A., Rijken, M., Wehunt, D., Chrusch, L., Ahmad, F., and Miskimins, J. 2021. Achieving near-uniform fluid and proppant placement in multistage fractured horizontal wells: A computational fluid dynamics modeling approach. SPE Production & Operations, 36:926–945.

Long, G., Liu, S., Xu, G., and Wong, S.-W. 2015. Modeling of perforation erosion for hydraulic fracturing applications. In Proceedings of the SPE Annual Technical Conference and Exhibition held in Houston, Texas, SPE-174959-MS.

Lorwongngam, Apiwat (Ohm), Shawn Wright, Stephanie Hari, Erin Butler, Michael McKimmy, Jennifer Wolters, and Craig Cipolla. 2020. Using multidisciplinary data gathering to evaluate eXtreme limited entry completion design and improve perforation cluster efficiency. In Proceedings of the Unconventional Resources Technology Conference and Exhibition, Austin, TX, URTeC-2796.

McClure, Mark, M.L. Albrecht, C. Bernet, C.L. Cipolla, K. Etcheverry, G. Fowler, A. Fuhr, A. Gherabati, M. Johnston, P. Kaufman, M. Mackay, M.P. McKimmy, C. Miranda, C. Molina, C.G. Ponners, D.R. Ratcliff, J. Rondon, A. Singh, R. Sinha, A. Sung, J. Xu, J. Yeo, R.B. Zinselmeyer. 2023. Results From a Collaborative Industry Study on Parent/Child Interactions. In Proceedings of the Hydraulic Fracturing Technology Conference and Exhibition, The Woodlands, TX, SPE-212321-MS.

Ngameni, K. L., Miskimins, J. L., Abass H. H., and Cherrian, B. 2017. Experimental study of proppant transport in horizontal wellbore using fresh water. In Proceedings of the Hydraulic Fracturing Technology Conference and Exhibition, The Woodlands, TX, SPE-184841-MS.

Robinson, Stephen, Thomas Littleford, Tim Luu, Kacper Wardynski, Andrew Evans, Blake Horton, and Michael Oman. 2020. Acoustic imaging of perforation erosion in hydraulically fractured wells for optimizing cluster efficiency. In Proceedings of the SPE Hydraulic Fracturing Technology Conference and Exhibition, The Woodlands, TX, SPE-199718-MS.

Sinkov., K., Weng, X., and Kresse, O. 2021. Modeling of Proppant Distribution During Fracturing of Multiple Perforation Clusters in Horizontal Wells. In Proceedings of SPE Hydraulic Fracturing Technology Conference and Exhibition, The Woodlands, TX , 204207-MS.

Snider, P., Baumgartner, S., Mayerhofer, M., and Woltz, M. 2022. Execution and learnings from the first two surface tests replicating unconventional fracturing and proppant transport. In Proceedings of the Hydraulic Fracturing Technology Conference, The Woodlands, TX, SPE- 209141-MS.

Wang, J., Singh, A., Liu, X., Rijken, M., Tan, Y., and Naik, S. 2022. Efficient prediction of proppant placement along a horizontal fracturing stage for perforation design optimization. SPE Journal, 27:1094–1108.

Weddle, Paul, Larry Griffin, and C. Mark Pearson. 2018. Mining the Bakken II – Pushing the envelope with extreme limited entry perforating. In Proceedings of the SPE Hydraulic Fracturing Technology Conference and Exhibition, The Woodlands, TX, SPE-189880-MS.

Wu, C.-H. and Sharma, M.M. 2016. Effect of perforation geometry and orientation on proppant placement in perforation clusters in a horizontal well. In Proceedings of the Hydraulic Fracturing Technology Conference, The Woodlands, TX, SPE-179117-MS.

Wu, C. 2018. Modeling Particulate Flows in Conduits and Porous Media. PhD thesis, University of Texas at Austin, Austin, TX.

Wu, C.-H. and Sharma, M.M. 2019. Modeling proppant transport through perforations in a horizontal wellbore. SPE Journal, 2:1777–1789, SPE-179117-PA.